



**HAL**  
open science

## IGF1 drives Wnt-induced joint damage and is a potential therapeutic target for osteoarthritis

Ana Escribano-Núñez, Frederique M F Cornelis, Astrid de Roover, An Sermon, Frédéric Cailotto, Rik J Lories, Silvia Monteagudo

### ► To cite this version:

Ana Escribano-Núñez, Frederique M F Cornelis, Astrid de Roover, An Sermon, Frédéric Cailotto, et al.. IGF1 drives Wnt-induced joint damage and is a potential therapeutic target for osteoarthritis. Nature Communications, 2024, 15 (1), pp.9170. 10.1038/s41467-024-53604-8 . hal-04759266

**HAL Id: hal-04759266**

**<https://hal.science/hal-04759266v1>**

Submitted on 29 Oct 2024

**HAL** is a multi-disciplinary open access archive for the deposit and dissemination of scientific research documents, whether they are published or not. The documents may come from teaching and research institutions in France or abroad, or from public or private research centers.

L'archive ouverte pluridisciplinaire **HAL**, est destinée au dépôt et à la diffusion de documents scientifiques de niveau recherche, publiés ou non, émanant des établissements d'enseignement et de recherche français ou étrangers, des laboratoires publics ou privés.



Distributed under a Creative Commons Attribution - NonCommercial - NoDerivatives 4.0 International License

# IGF1 drives Wnt-induced joint damage and is a potential therapeutic target for osteoarthritis

Received: 21 March 2024

Accepted: 14 October 2024

Published online: 24 October 2024

 Check for updates

Ana Escribano-Núñez<sup>1</sup>, Frederique M. F. Cornelis<sup>1</sup>, Astrid De Roover<sup>1</sup>, An Sermon<sup>2,3</sup>, Frédéric Cailotto<sup>4</sup>, Rik J. Lories<sup>1,5,6</sup> & Silvia Monteagudo<sup>1,6</sup> ✉

Osteoarthritis is the most common joint disease and a global leading cause of pain and disability. Current treatment is limited to symptom relief, yet there is no disease-modifying therapy. Its multifactorial etiology includes excessive activation of Wnt signaling, but how Wnt causes joint destruction remains poorly understood. Here, we identify that Wnt signaling promotes the transcription of insulin-like growth factor 1 (IGF1) in articular chondrocytes and that IGF1 is a major driver of Wnt-induced joint damage. Male mice with cartilage-specific *Igf1* deficiency are protected from Wnt-triggered joint disease. Mechanistically, Wnt-induced *IGF1* transcription depends on  $\beta$ -catenin and binding of Wnt transcription factor TCF4 to the *IGF1* gene promoter. In a clinically relevant mouse model of post-traumatic osteoarthritis, cartilage-specific deletion of *Igf1* protects against the disease in male mice. *IGF1* silencing in chondrocytes from patients with osteoarthritis restores a healthy molecular profile. Our findings reveal that reducing Wnt-induced IGF1 is a potential therapeutic strategy for osteoarthritis.

Osteoarthritis, the most common chronic joint disease affecting more than 500 million people (7% of the global population), is characterized by progressive joint damage, which leads to pain and loss of function<sup>1</sup>. The prevalence and burden associated with the disease are steadily increasing due to the aging of the population and rising obesity rates. This represents a major escalating public health challenge for the decades ahead. Osteoarthritis, ranked as a major contributor to global disability and chronic pain, adversely affects mobility, physical function, and individual well-being<sup>1</sup>. The currently available pharmacological treatments are only able to target the disease symptoms and, in severe cases, joint replacement surgery is the only option. The absence of an effective disease-modifying therapy has led to the recognition of osteoarthritis as a serious disease with a high unmet medical need<sup>2</sup>.

Osteoarthritis is a complex disease that affects the whole joint. It is primarily characterized by articular cartilage damage and is often accompanied by osteophyte formation, subchondral bone sclerosis, and synovial inflammation. Similarly to many common diseases, the etiology of osteoarthritis is complex, involving multiple factors that contribute to the condition. These factors include joint injury, altered joint anatomy and biomechanics, aging, obesity, and metabolic alterations, all of which interact with the individual's genetic predisposition<sup>3</sup>. The multifactorial nature of the disease combined with the multiple alterations in distinct joint tissues may explain why the development of an effective therapy for osteoarthritis remains a major challenge.

<sup>1</sup>Laboratory of Tissue Homeostasis and Disease, Skeletal Biology and Engineering Research Centre, Department of Development and Regeneration, KU Leuven, Leuven, Belgium. <sup>2</sup>Division of Trauma Surgery, University Hospitals Leuven, Leuven, Belgium. <sup>3</sup>Locomotor and Neurological Disorders Unit, Department of Development and Regeneration, KU Leuven, Leuven, Belgium. <sup>4</sup>CNRS-University of Lorraine, Molecular Engineering and Articular Physiology, Biopôle, University of Lorraine; Campus Biologie-Santé, Vandœuvre-Lès-Nancy, France. <sup>5</sup>Division of Rheumatology, University Hospitals Leuven, Leuven, Belgium. <sup>6</sup>These authors contributed equally: Rik J. Lories, Silvia Monteagudo. ✉e-mail: [silvia.monteagudo@kuleuven.be](mailto:silvia.monteagudo@kuleuven.be)

A detailed understanding of the mechanisms underlying the initiation and progression of osteoarthritis is crucial to identify effective targets and strategies. Hyper-activation of canonical  $\beta$ -catenin-dependent Wnt signaling (henceforth referred to as Wnt signaling for brevity) has been strongly implicated in the pathogenesis of the disease<sup>4,5</sup>. Wnt signaling is highly conserved and versatile, regulating tissue development, homeostasis, and disease, and has been increasingly recognized as a therapeutic target for osteoarthritis<sup>5,6</sup>. However, the downstream molecular players that drive Wnt-induced damage to the joint remain elusive, posing a substantial barrier to the development of highly specific and effective pharmacological interventions.

Here, we analyzed two different genome-wide transcriptome datasets of articular cartilage with Wnt hyper-activation and unraveled that Wnt signaling promotes the expression of insulin-like growth factor 1 (IGF1) in chondrocytes. Then, using mice with cartilage-specific *Igf1* deficiency, we demonstrate that IGF1 drives joint damage downstream of Wnt activation. We identify the underlying molecular mechanisms that involve direct transcriptional control of IGF1 by Wnt signaling. Translationally, we prove that suppression of IGF1 in articular cartilage protects against osteoarthritis in mice upon joint injury and restores a healthy molecular profile in chondrocytes from patients with osteoarthritis. Our findings therefore indicate that decreasing Wnt-induced IGF1 may represent a therapeutic strategy for osteoarthritis.

## Results

### Bioinformatics reveal a Wnt-IGF1 link in articular cartilage

To identify key downstream molecular players that drive the deleterious effects of excessive Wnt signaling activation in osteoarthritis, we took advantage of our genome-wide transcriptome dataset from human articular chondrocytes (hACs) wherein we inhibited the activity of the *Disruptor of telomeric silencing-1 like* (DOT1L) enzyme (geonr: GSE77916)<sup>7</sup>. In chondrocytes, Wnt signaling is epigenetically restricted by DOT1L, a histone methyltransferase that maintains joint homeostasis<sup>7,8</sup>. DOT1L inhibition in these cells thus resulted in hyper-activation of Wnt signaling<sup>7</sup>. We performed a protein network analysis of the top up- and down-regulated genes in the transcriptome dataset using db-STRING<sup>9</sup>. This analysis defined a transcriptional network with IGF1 as a prominent node (Fig. 1a), suggesting a regulatory loop in articular cartilage that links Wnt hyper-activation with IGF1. In fact, *IGF1* appeared among the top upregulated genes in the transcriptome dataset (geonr: GSE77916). In addition, we performed network analysis using the HumanBase tool, which allows us to build cartilage-specific networks<sup>10</sup>. This analysis revealed that both Wnt and IGF1 pathways appeared as major cartilage-specific modules, likewise suggesting a connection between these two signaling cascades (Fig. 1b and Supplementary Table 1). Up-regulation of *IGF1* expression in DOT1L-inhibited hACs was experimentally validated by quantitative PCR (Fig. 1c). In vivo, we detected increased IGF1 protein levels in articular cartilage of mice intra-articularly injected with a DOT1L inhibitor (Fig. 1d) and of cartilage-specific *Dot1l* knockout (KO) mice compared to controls (Supplementary Fig. 1a, b), a pattern similar to that of the direct Wnt target gene *TCF1*<sup>7,8</sup>. Thus, loss of the negative epigenetic Wnt regulator DOT1L and subsequent Wnt hyper-activation trigger IGF1 expression in articular cartilage.

Then, we analyzed a different in vivo model of Wnt gain-of-function, the *Frizzled-related-protein* (*Frzb*) KO mice. FRZB, also called secreted Frizzled-related protein 3 (sFRP3), is an extracellular antagonist in the Wnt signaling pathway. *Frzb* KO mice display more articular cartilage damage compared to controls in osteoarthritis triggered by surgical instability, enzymatic injury, or inflammation, associated with increased Wnt signaling<sup>11,12</sup>. We found that, in our previous transcriptome dataset of articular cartilage of *Frzb* KO mice compared to wild-type mice (geonr: GSE33656)<sup>13</sup>, *Igf1* expression was highly upregulated. Network analysis of this transcriptome dataset

using db-STRING showed IGF1 as a highly connected node (Fig. 1e). We also examined this dataset using the HumanBase tool and identified Wnt signaling as one of the major cartilage-specific modules. Within this module, IGF1 appeared as a central node (Fig. 1f and Supplementary Table 2). We detected increased IGF1 expression in the articular cartilage of *Frzb* KO mice (Fig. 1g), comparable to staining for the direct Wnt target gene *TCF1* (Supplementary Fig. 2a). Together, these results show that loss of Wnt negative regulators acting at different molecular levels increases IGF1 in articular cartilage, suggesting an intriguing link between Wnt signaling activation and IGF1 expression in this tissue.

IGF1 is a protein that is critical for normal body development, growth, and maintenance<sup>14</sup>. In growth plate cartilage, a transient tissue that is gradually replaced by bone during skeletal development and growth, IGF1 stimulates chondrocyte hypertrophy, promoting bone growth before and after birth<sup>15,16</sup>. Due to this anabolic role, IGF1 has been explored in tissue engineering approaches toward joint repair<sup>17</sup>. However, recent evidence has shown that IGF1 can trigger aberrant chondrocyte hypertrophy in bovine articular chondrocytes<sup>18</sup> and in the human costal C28/I2 chondrocyte cell line<sup>19</sup>, thereby changing the cells' molecular identity. Of note, we found multiple lines of experimental evidence that IGF1 expression is upregulated in osteoarthritic articular cartilage, serum, and synovial fluid from different species, including humans (Supplementary Table 3). Despite these observations, the precise role of IGF1 in osteoarthritis remains largely elusive, primarily due to the absence of studies employing cartilage-specific *Igf1*-deficient animals in translational models of the disease. In addition, the signaling pathways that control the expression of IGF1 in articular chondrocytes are unknown.

### Wnt signaling induces IGF1 in articular chondrocytes

Following the intriguing observations in the different models of Wnt negative regulators, we proceeded to examine the impact of direct activation of Wnt signaling on the expression of IGF1 in articular cartilage. To this end, we treated hACs with recombinant WNT3A, which binds Frizzled receptors and the low-density lipoprotein receptor-related protein (LRP) 5 and 6 coreceptors and activates canonical Wnt signaling. WNT3A increased *IGF1* gene expression in a concentration-dependent manner (Fig. 2a), similar to the effect on Wnt target gene *TCF1* (Supplementary Fig. 2b).

Glycogen synthase kinase-3 $\beta$  (GSK-3 $\beta$ ) is a key component in the canonical Wnt signaling cascade, as part of a cytosolic destruction complex that targets  $\beta$ -catenin for proteasomal degradation, thereby antagonizing Wnt signaling. To further investigate the effects of Wnt signaling activation on IGF1 expression, we tested two different pharmacological GSK-3 $\beta$  inhibitors, the ATP-competitive inhibitor CHIR-99021 (CHIR) and the non-ATP-competitive inhibitor lithium chloride (LiCl). Both CHIR and LiCl treatments upregulated *IGF1* gene expression in a concentration-dependent manner in hACs (Fig. 2b, c), similar to the effect on *TCF1* (Supplementary Fig. 2c, d).

The *IGF1* gene can be the origin of distinct transcripts that encode for different precursor polypeptides<sup>20</sup> (Supplementary Fig. 3a). Only *IGF1* class 1 transcripts were found in hACs, and all the class 1 transcripts were enhanced upon Wnt stimulation (Supplementary Fig. 3b-d). Of note, Wnt signaling activation by WNT3A or GSK-3 $\beta$  inhibitors did not change the expression of paralog gene *IGF2* (Supplementary Fig. 4a-c).

Then, we tested whether Wnt signaling activation also leads to enhanced IGF1 protein levels. We used an in vitro enzyme-linked immunosorbent assay (ELISA) for the quantitative measurement of IGF1 in cell culture supernatants of hACs treated with different concentrations of WNT3A, CHIR, and LiCl. Wnt activation led to a concentration-dependent up-regulation of IGF1 protein amounts (Fig. 2d-f). In vivo, intra-articular injections of Wnt activator CHIR in wild-type mice also resulted in enhanced IGF1 protein amounts in articular cartilage (Fig. 2g) mirroring the increase in *TCF1*

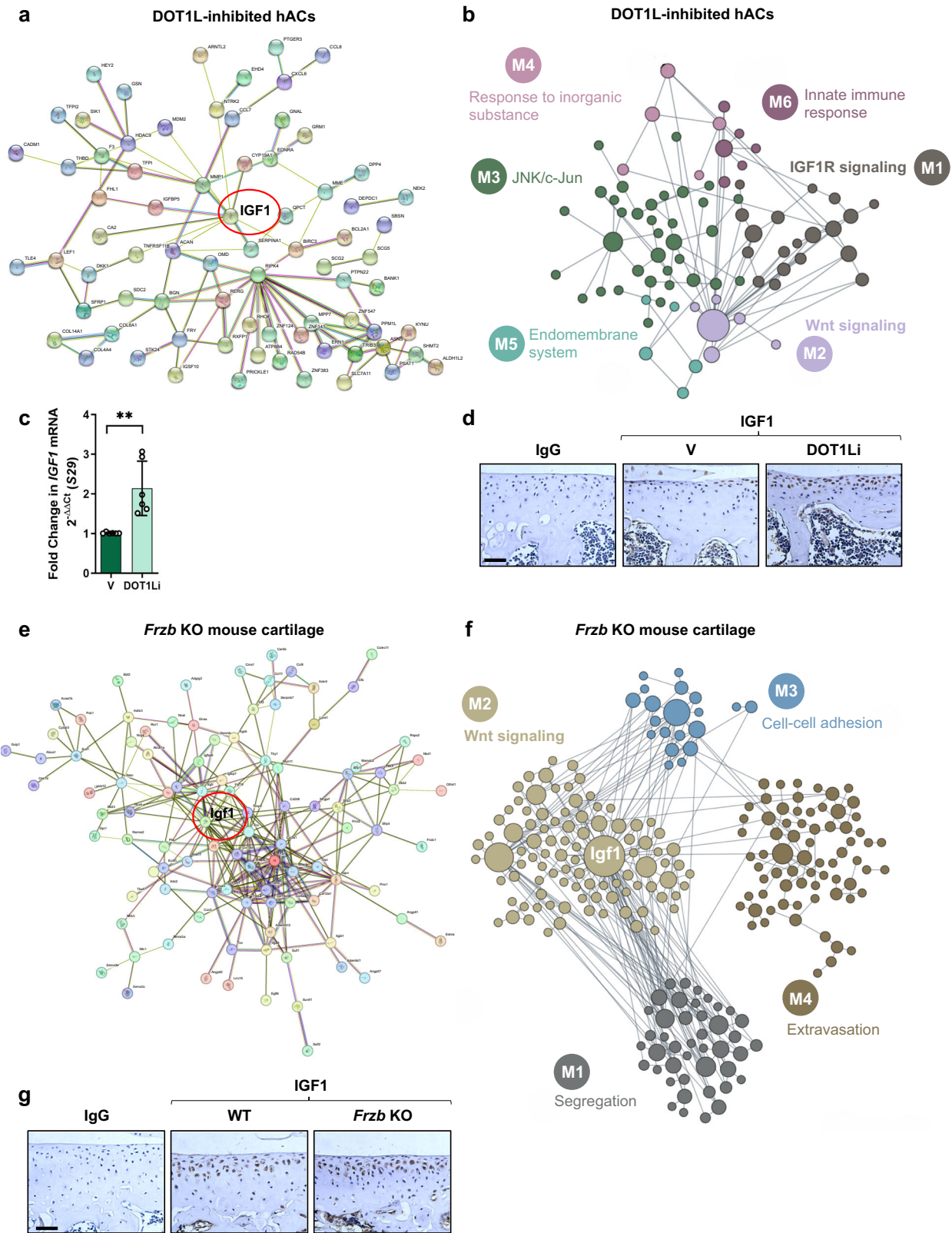


**Fig. 1 | Bioinformatic analysis and validation experiments reveal a link between Wnt signaling and IGF1 in articular cartilage and osteoarthritis.** **a, b** STRINGdb protein-protein network (a) and HumanBase cartilage-specific network (b) of top differentially expressed genes in microarray data obtained from human articular chondrocytes (hACs) treated with DOT1L inhibitor (DOT1Li) EPZ-5676 or vehicle (V) ( $n = 5$  different donors). **c** Real-time PCR of *IGF1* gene expression in hACs treated with DOT1Li or V ( $n = 6$  different donors with 3 technical replicates per donor),  $**t_5 = 5.5$ ,  $p = 0.0027$  by two-sided paired  $t$ -test. Error bars indicate mean  $\pm$  SD. Source data are

provided as a Source Data file. **d** Immunohistochemical detection of IGF1 in articular cartilage of 10-week-old male wild-type (WT) mice treated with DOT1Li or V (images are representative of 3 mice per group). Scale bar: 50  $\mu$ m. **e, f** STRINGdb protein-protein network (e) and HumanBase cartilage-specific network (f) of top differentially expressed genes in microarray data comparing articular cartilage of 6-week-old male *Frzb* knockout (KO) mice to WT mice ( $n = 3$  mice per group). **g** Immunohistochemical detection of IGF1 in articular cartilage of 8-week-old male *Frzb* KO or WT mice (images are representative of 3 mice per group). Scale bar: 50  $\mu$ m.

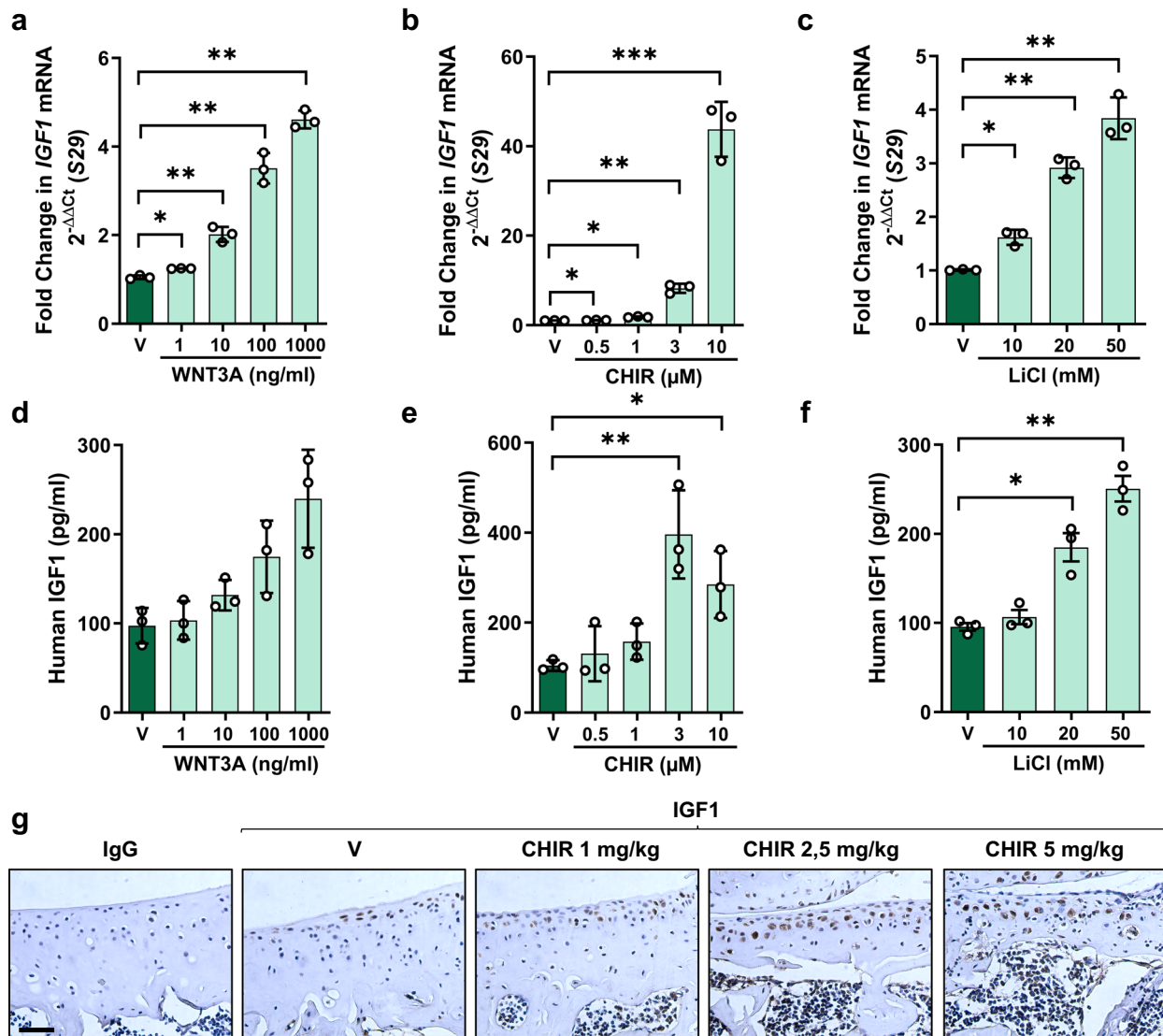


**Fig. 2 | Wnt signaling activation induces IGF1 expression in articular chondrocytes.** **a–c** Real-time PCR of *IGF1* gene expression in human articular chondrocytes (hACs) treated with vehicle (V), WNT3A (**a**), CHIR-99021 (CHIR) (**b**) or Lithium Chloride (LiCl) (**c**). **d–f** Protein levels of IGF1 in hACs treated with V, WNT3A (**d**), CHIR (**e**), or LiCl (**f**) as determined by ELISA. **a–f**  $n = 3$  different donors with 3 technical replicates per donor.  $F_{1,202, 2,403} = 429.2$ ,  $*p = 0.0432$  (V vs WNT3A 1 ng/ml),  $**p = 0.0036$  (V vs WNT3A 10 ng/ml),  $**p = 0.0017$  (V vs WNT3A 100 ng/ml),  $**p = 0.0017$  (V vs WNT3A 100 ng/ml) (**a**);  $F_{1,459, 2,918} = 1923$ ,  $*p = 0.0396$  (V vs CHIR 0.5  $\mu$ M),  $*p = 0.0120$  (V vs CHIR 1  $\mu$ M),  $**p = 0.0019$  (V vs CHIR 3  $\mu$ M),  $***p = 0.0008$

(V vs CHIR 10  $\mu$ M) (**b**);  $F_{1,842, 3,684} = 342.4$ ,  $*p = 0.0204$  (V vs LiCl 10 mM),  $**p = 0.0019$  (V vs LiCl 20 mM),  $**p = 0.0037$  (V vs LiCl 50 mM) (**c**);  $F_{1,050, 2,100} = 21.70$  (**d**);  $F_{1,022, 2,044} = 11.34$ ,  $**p = 0.0067$  (V vs CHIR 3  $\mu$ M),  $*p = 0.0195$  (V vs CHIR 10  $\mu$ M) (**e**);  $F_{1,129, 2,258} = 75.04$ ,  $*p = 0.119$  (V vs LiCl 20 mM),  $**p = 0.0081$  (V vs LiCl 50 mM) (**f**) in repeated measures one-way ANOVA for 4 (**a, b, d, e**) or 3 (**c, f**) pairwise tests using the Dunnett's multiple comparisons test. Error bars indicate mean  $\pm$  SD. Source data are provided as a Source Data file. **g** Immunohistochemical detection of IGF1 in articular cartilage of 9-week-old male wild-type mice treated with the indicated doses of CHIR or V (images are representative of 3 mice per group). Scale bar: 50  $\mu$ m.

(Supplementary Fig. 2e). Thus, Wnt signaling activation increases IGF1 expression both at the transcriptional and at the protein level, in articular chondrocytes.

Growth hormone (GH), the main inducer of IGF1 in the liver, which accounts for 75% of circulating IGF1<sup>14</sup>, did not induce IGF1 expression in hACs (Supplementary Fig. 5a), in agreement with previous observations<sup>21</sup>. In C2C12 muscle cells, used as a positive control, GH did induce IGF1 expression (Supplementary Fig. 5b). Therefore, GH-independent mechanisms, in particular Wnt signaling, seem to be key for controlling local IGF1 expression in articular cartilage.

### IGF1 is a key downstream player in Wnt-triggered joint damage

We next sought to elucidate the biological significance of the identified Wnt/IGF1 link in articular cartilage and osteoarthritis. To this end, we

generated inducible cartilage-specific *Igf1* KO (*Igf1*<sup>CART-KO</sup>) male mice. Four weeks after injection of tamoxifen to trigger recombination in chondrocytes, IGF1 expression was strongly reduced in articular cartilage of *Igf1*<sup>CART-KO</sup> mice compared to controls, validating the efficiency of the KO technique (Supplementary Fig. 6a, b). To determine the effects of IGF1 downstream of Wnt signaling in the joint, we locally induced Wnt signaling hyper-activation by repeated intra-articular injections of CHIR in *Igf1*<sup>CART-KO</sup> and control mice (Fig. 3a). After Wnt hyper-activation with CHIR, *Igf1*<sup>CART-KO</sup> presented less cartilage damage compared to control mice, suggesting that deletion of the *Igf1* gene upon Wnt activation protects against the development of osteoarthritis (Fig. 3b). *Igf1*<sup>CART-KO</sup> also showed less osteophyte formation compared to controls upon Wnt activation with CHIR (Fig. 3c). Hyper-activation of Wnt signaling in the joint led to mildly increased synovial

inflammation in both *Igfl1*<sup>CART-KO</sup> mice and control mice (Supplementary Fig. 7a). Although the difference was not statistically significant, a trend toward less synovial inflammation in *Igfl1*<sup>CART-KO</sup> mice compared to controls was observed. In addition, we measured the subchondral bone plate thickness of the tibial plateau of the mice by histomorphometry. *Igfl1*<sup>CART-KO</sup> mice presented increased subchondral bone thickness compared to control mice in the vehicle group. However, the subchondral bone thickness was decreased in *Igfl1*<sup>CART-KO</sup> mice upon Wnt activation but not in control mice (Supplementary Fig. 7b).

In osteoarthritis, articular chondrocytes lose their molecular identity and aberrantly differentiate toward hypertrophic chondrocytes<sup>22</sup>. This switch contributes to joint damage and has been associated with increased Wnt signaling<sup>4</sup>. In line with this, we detected increased chondrocyte hypertrophy in the articular cartilage of control mice intra-articularly injected with CHIR, assessed by immunohistochemistry of chondrocyte hypertrophy marker collagen type 10 (COLX). Cartilage-specific deletion of *Igfl1* prevented pathological hypertrophic differentiation upon Wnt hyper-activation (Fig. 3d). Furthermore, we detected neopeptides of aggrecan degradation using NITEGE staining. Deletion of the *Igfl1* gene in the articular cartilage of *Igfl1*<sup>CART-KO</sup> mice prevented the increase in aggrecan degradation observed after intra-articular injections of CHIR in control mice (Fig. 3e). We further assessed the effects of deleting *Igfl1* in articular cartilage from mice by performing immunohistochemistry of different matrix-degrading enzymes. *Igfl1*<sup>CART-KO</sup> presented less staining of the cartilage degrading enzymes matrix metalloproteinase 13 (MMP13) and a disintegrin and metalloproteinase with thrombospondin motifs 5 (ADAMTS5) compared to control mice upon CHIR intra-articular injections (Supplementary Fig. 8a, b). These results indicate that *Igfl1* deletion in articular cartilage protects mice from developing Wnt-triggered osteoarthritic changes. Thus, IGF1 acts as a key downstream molecular player in the deleterious cascade of events triggered by Wnt signaling in the joint.

### IGF1 is a direct Wnt target gene in articular chondrocytes

Considering the important role of IGF1 in the development of Wnt-triggered osteoarthritis, we investigated the molecular mechanisms via which Wnt regulates IGF1 expression. First, we explored the role of the central canonical Wnt signaling component  $\beta$ -catenin. To this end, we initially used the in vivo model of epigenetically-driven Wnt hyper-activation by DOT1L inhibition in articular cartilage, as these mice showed increased IGF1 expression (Fig. 1d). To determine whether the latter effect is  $\beta$ -catenin-dependent, we analyzed knee sections of mice that we previously intra-articularly co-injected with a DOT1L inhibitor and Wnt inhibitor XAV-939 (XAV)<sup>7</sup>. The tankyrase inhibitor XAV stimulates  $\beta$ -catenin degradation by stabilizing Axin, the concentration-limiting component of the destruction complex. XAV co-administration prevented up-regulation of IGF1 expression in this Wnt hyper-activation model (Fig. 4a). To validate the involvement of  $\beta$ -catenin in the induction of IGF1 expression, we silenced  $\beta$ -catenin in hACs and treated these cells with WNT3A to stimulate Wnt signaling. We observed that siRNA-mediated knockdown of  $\beta$ -catenin blocked WNT3A-induced *IGF1* expression (Fig. 4b and Supplementary Fig. 9a). These results demonstrate that induction of *IGF1* expression upon Wnt signaling activation is  $\beta$ -catenin-dependent.

Next, we investigated whether Wnt signaling directly regulates the transcription of the *IGF1* gene in articular chondrocytes. To this end, we first performed a luciferase reporter assay. We cloned the full *IGF1* promoter (-1999 bp to +100 bp relative from the transcription start site [TSS]) into the pGL3-basic vector upstream of a reporter luciferase gene. This plasmid was transfected into hACs followed by WNT3A treatment. Luciferase activity was increased in cells transfected with the *IGF1* promoter construct upon Wnt activation with WNT3A, compared with unstimulated and empty construct control conditions (Fig. 4c). These results evidence that Wnt

signaling transcriptionally induces *IGF1* expression in articular chondrocytes.

$\beta$ -catenin does not directly bind to DNA but regulates transcription via interaction with T-cell factor/Lymphoid-enhancing factor (TCF/LEF) transcription factors. We examined the presence of TCF/LEF response elements<sup>23</sup> in the *IGF1* gene promoter. We found putative binding sites for Wnt TCF/LEF transcription factors, including one consensus binding site that was highly conserved among different species, from zebrafish to humans (Fig. 4d and Supplementary Fig. 10). Additionally, some TCF transcription factors also have a second DNA binding domain called C-clamp, which recognizes a motif termed helper site that contributes to the control of specific Wnt target genes' expression<sup>24</sup>. We also found a helper site in the *IGF1* gene promoter, which was highly conserved among species (Supplementary Fig. 10 and Supplementary Fig. 11). Then, we investigated whether TCF/LEF factors directly bind to the *IGF1* gene promoter, using chromatin immunoprecipitation (ChIP)-qPCR analysis in hACs. Most vertebrates have four members of the TCF/LEF family: TCF1, TCF3, TCF4 and LEF1<sup>23</sup>. TCF4 is the most abundant TCF family member in human cartilage<sup>25</sup>. We observed TCF4 binding to the *IGF1* gene promoter upon Wnt pathway activation (Fig. 4e). Conversely, TCF3 bound to the *IGF1* gene promoter under basal conditions, and was released from the chromatin upon Wnt pathway activation (Fig. 4e), suggesting a TCF switch mechanism<sup>23</sup>. A similar TCF binding pattern was found for the *TCF1* gene promoter (Supplementary Fig. 12). *TCF4* silencing using siRNA appeared to block Wnt-induced up-regulation of *IGF1* in hACs (Fig. 4f and Supplementary Fig. 9b). Thus, TCF4 is a positive regulator of *IGF1* gene expression in articular chondrocytes. In contrast, silencing of *TCF3* in basal conditions led to an up-regulation in *IGF1* expression (Fig. 4g and Supplementary Fig. 9c). These data suggest that, in basal conditions, TCF3 represses *IGF1* expression in articular chondrocytes and, upon Wnt signaling activation, TCF3 is replaced by TCF4 (Fig. 4h). In addition, activation of Wnt signaling increased histone marks associated with greater accessibility of the chromatin for active transcription in the *IGF1* promoter, namely acetylation of H3K9 and trimethylation of H3K4 (Fig. 4i). Altogether, these results demonstrate that IGF1 is a direct Wnt target gene in articular chondrocytes.

To explore the potential scope of the identified Wnt/IGF1 molecular mechanism in other tissues, we interrogated IGF1 as a potential target gene of TCF/LEF transcription factors using the ChIP-Atlas database<sup>26</sup>, an integrative and comprehensive data-mining suite of public ChIP-Seq data. This analysis revealed high MACS2 scores for TCF4, TCF3, and TCF1 in different cell types, indicating a high binding to the *IGF1* promoter (Fig. 4j). In line with these observations, exploratory experiments showed that Wnt signaling activation induced *IGF1* gene expression in primary human osteoblasts and primary human skin fibroblasts (Supplementary Fig. 13a, b). Thus, Wnt signaling seems to control IGF1 expression also in other cell types beyond the articular chondrocyte.

### *Igfl1* deletion in cartilage protects mice against osteoarthritis

Next, we investigated the translational implications of the identified direct Wnt/IGF1 link in a clinically relevant animal model of osteoarthritis. We evaluated the impact of cartilage-specific deletion of *Igfl1* in the destabilization of the medial meniscus (DMM) mouse model<sup>27</sup>, which mimics features of human post-traumatic osteoarthritis. In the DMM model, Wnt signaling is upregulated in the joint after injury<sup>28</sup>. DMM or sham surgery was performed 1 week after tamoxifen injection in *Igfl1*<sup>CART-KO</sup> male mice and control mice, and knee joints were collected 12 weeks after surgery (Fig. 5a). Cartilage damage, as indicative of disease severity, was reduced in DMM-operated *Igfl1*<sup>CART-KO</sup> mice compared to DMM-operated controls (Fig. 5b). Osteophyte formation was also reduced in DMM-operated *Igfl1*<sup>CART-KO</sup> mice compared to DMM-operated controls (Fig. 5c). Synovial inflammation was low after DMM

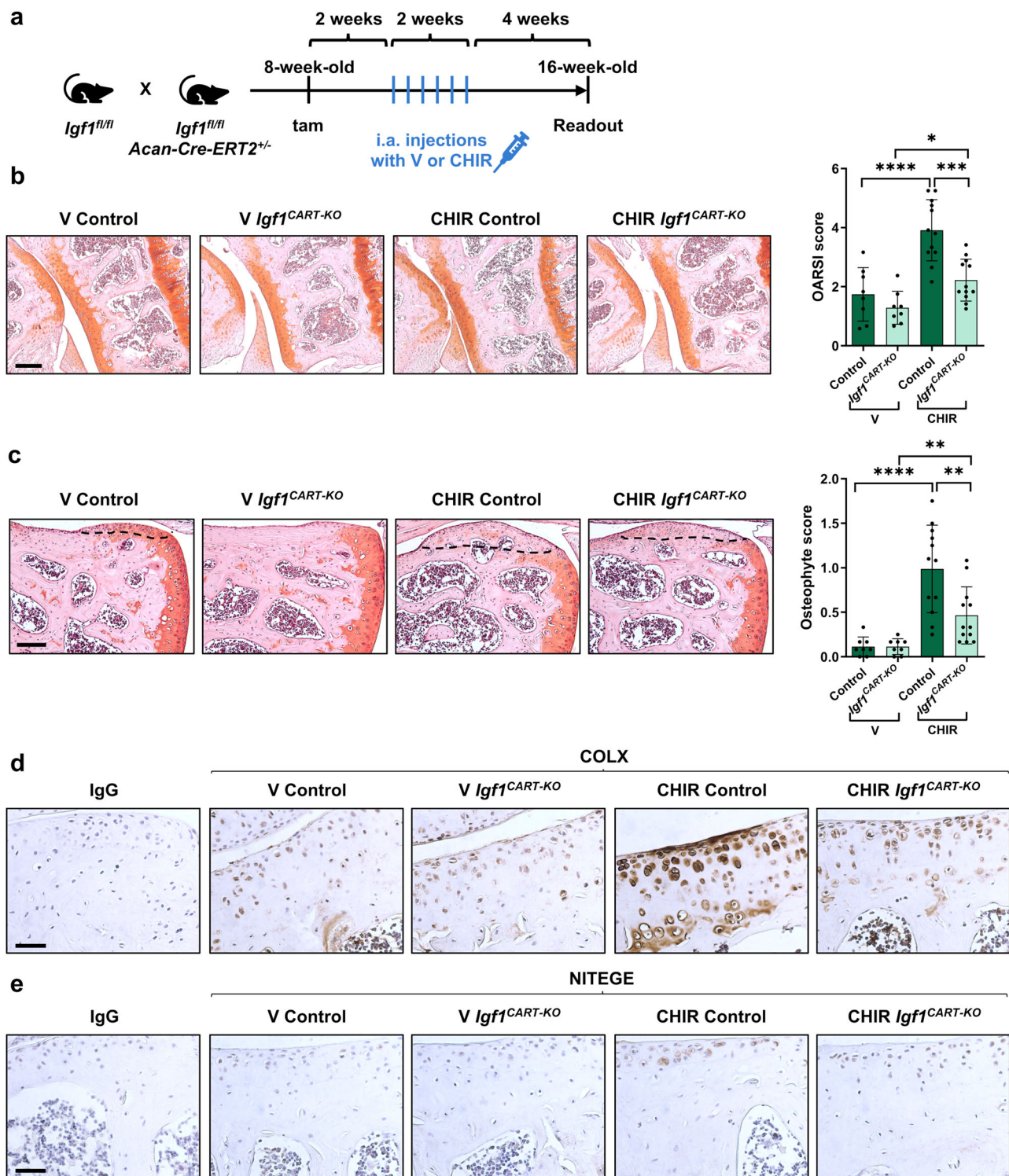
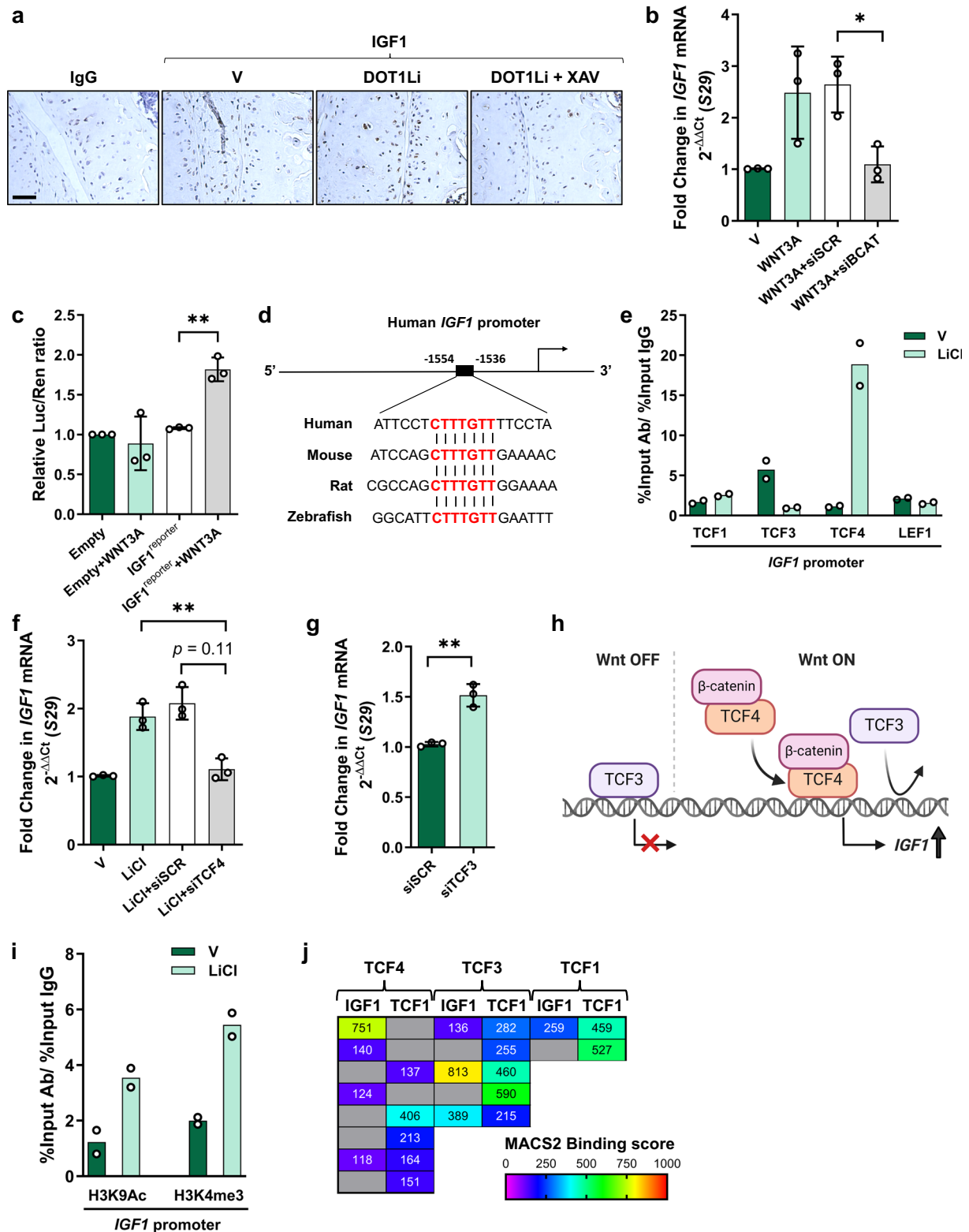


**Fig. 3 | Cartilage-specific deletion of *Igf1* protects against osteoarthritis upon Wnt signaling activation in mice.** **a** Schematic outline of intra-articular injections of CHIR-99021 (CHIR) or vehicle (V) after postnatal deletion of *Igf1* in male *Igf1<sup>CART-KO</sup>* mice. *Igf1<sup>fl/fl</sup>* mice were bred to *Igf1<sup>fl/fl</sup>; Aggrecan-Cre<sup>ERT2</sup>* mice and treated with tamoxifen. Tamoxifen-treated *Igf1<sup>fl/fl</sup>* mice served as controls. **b** Frontal haematoxylin-safranin O staining of the lateral tibia and femur and quantification of articular cartilage damage at the 4 quadrants, evaluated by OARS1 score [ $n = 8$  (V control and V *Igf1<sup>CART-KO</sup>*),  $n = 12$  (CHIR control and CHIR *Igf1<sup>CART-KO</sup>*)],  $F_{1,36} = 49.1, 4.329, 4.631$  for treatment, genotype and interaction, respectively, in two-way ANOVA,  $*p = 0.0401$  (V *Igf1<sup>CART-KO</sup>* vs CHIR *Igf1<sup>CART-KO</sup>*),  $***p = 0.0007$  (CHIR control vs CHIR *Igf1<sup>CART-KO</sup>*),  $****p < 0.0001$  (V control vs CHIR control) for 6 pairwise tests using the Sidák multiple comparisons test. Error bars indicate mean  $\pm$  SD. Scale bar: 200  $\mu$ m. **c** Frontal haematoxylin-safranin O staining of the medial femur and quantification of osteophytes at the 4 quadrants [ $n = 8$  (V control and V *Igf1<sup>CART-KO</sup>*),  $n = 12$  (CHIR control and CHIR *Igf1<sup>CART-KO</sup>*)],  $F_{1,36} = 49.1, 4.329, 4.631$  for treatment, genotype and interaction, respectively, in two-way ANOVA,  $*p = 0.0401$  (V *Igf1<sup>CART-KO</sup>* vs CHIR *Igf1<sup>CART-KO</sup>*),  $***p = 0.0007$  (CHIR control vs CHIR *Igf1<sup>CART-KO</sup>*),  $****p < 0.0001$  (V control vs CHIR control) for 6 pairwise tests using the Sidák multiple comparisons test. Error bars indicate mean  $\pm$  SD. Scale bar: 100  $\mu$ m. **b, c** Source data are provided as a Source Data file. **d, e** Immunohistochemical detection of chondrocyte hypertrophy marker collagen type 10 (COLX) (**d**) and aggrecan degradation marker NITEGE (**e**) in articular cartilage of *Igf1<sup>CART-KO</sup>* and control mice upon Wnt hyper-activation triggered by CHIR intra-articular injections, compared with mice intra-articularly injected with V (images are representative of 5 mice per group). Scale bar: 50  $\mu$ m.

200  $\mu$ m. **c** Frontal haematoxylin-safranin O staining of the medial femur and quantification of osteophytes at the 4 quadrants [ $n = 8$  (V control and V *Igf1<sup>CART-KO</sup>*),  $n = 12$  (CHIR control and CHIR *Igf1<sup>CART-KO</sup>*)],  $F_{1,36} = 49.1, 4.329, 4.631$  for treatment, genotype and interaction, respectively, in two-way ANOVA,  $*p = 0.0401$  (V *Igf1<sup>CART-KO</sup>* vs CHIR *Igf1<sup>CART-KO</sup>*),  $***p = 0.0007$  (CHIR control vs CHIR *Igf1<sup>CART-KO</sup>*),  $****p < 0.0001$  (V control vs CHIR control) for 6 pairwise tests using the Sidák multiple comparisons test. Error bars indicate mean  $\pm$  SD. Scale bar: 100  $\mu$ m. **b, c** Source data are provided as a Source Data file. **d, e** Immunohistochemical detection of chondrocyte hypertrophy marker collagen type 10 (COLX) (**d**) and aggrecan degradation marker NITEGE (**e**) in articular cartilage of *Igf1<sup>CART-KO</sup>* and control mice upon Wnt hyper-activation triggered by CHIR intra-articular injections, compared with mice intra-articularly injected with V (images are representative of 5 mice per group). Scale bar: 50  $\mu$ m.



surgery in both control and *Igf1*<sup>CART-KO</sup> mice and there were no significant differences between both genotypes (Supplementary Fig. 14a). We also measured the subchondral bone plate thickness of the tibial plateau of DMM-induced and sham-operated mice by histomorphometry. There were no differences in the extent of subchondral bone remodeling between the genotypes (Supplementary Fig. 14b).

DMM-operated *Igf1*<sup>CART-KO</sup> mice presented fewer hypertrophic chondrocytes in the articular cartilage than DMM-operated control mice, as indicated by COLX immunohistochemistry (Fig. 5d).

Additionally, deletion of *Igf1* in the cartilage of DMM-operated mice suppressed aggrecan degradation, indicated by reduced immunohistochemical staining of NITEGE, a disease feature that was more present in DMM-operated control mice (Fig. 5e). *Igf1*<sup>CART-KO</sup> also presented less staining of the cartilage degrading enzymes MMP13 and ADAMTS5 compared to control mice, upon DMM (Supplementary Fig. 15a, b). These in vivo data indicate that upon joint injury, deletion of *Igf1* in articular cartilage protects male mice against osteoarthritis.

**Fig. 4 | IGF1 is a direct Wnt target gene in articular chondrocytes.**

**a** Immunohistochemistry of IGF1 in articular cartilage of wild-type male mice treated with DOT1L inhibitor (DOT1Li), XAV-939 (XAV), or vehicle (V) (images are representative of 3 mice per group). Scale bar: 50  $\mu$ m. **b** Real-time PCR of *IGF1* expression in human articular chondrocytes (hACs) transfected with  $\beta$ -catenin (siBCAT) or scrambled (siSCR) siRNA for 48 h, followed by WNT3A treatment (100 ng/ml) for 24 h,  $F_{1,435,2,870} = 22.50$ ,  $*p = 0.387$ , Šidák corrected for 3 tests by repeated measures one-way ANOVA. **c** Luciferase assay in hACs transfected with empty plasmid or IGF1 promoter reporter, upon WNT3A treatment (100 ng/ml) for 24 h, normalized to Renilla, relative to empty plasmid,  $F_{1,4} = 2.93, 15.85, 10.65$  for plasmid, treatment and interaction, respectively,  $**p = 0.0018$ , Šidák corrected for 2 tests by repeated measures two-way ANOVA. **d** Scheme of *IGF1* promoter showing the location and sequence of the TCF/LEF consensus binding site in different species. **e** Chromatin immunoprecipitation (ChIP)-qPCR for TCF1, TCF3, TCF4, and LEF1 binding to *IGF1* promoter in hACs upon Wnt activation with LiCl (20 mM) for

24 h. **f** Real-time PCR of *IGF1* expression in hACs transfected with TCF4 (siTCF4) or siSCR siRNA for 48 h, followed by 24 h treatment with LiCl (20 mM),  $F_{1,111,2,221} = 38.05$ ,  $**p = 0.0050$ , Šidák corrected for 3 tests by repeated measures one-way ANOVA. **g** Real-time PCR of *IGF1* expression in hACs transfected with TCF3 (siTCF3) or siSCR siRNA for 48 h,  $**t_2 = 12.54$ ,  $p = 0.0063$  by two-sided paired *t*-test. **h** Scheme of the proposed TCF switch mechanism controlling *IGF1* expression. TCF3 represses *IGF1* in basal conditions and is replaced by TCF4 upon Wnt activation. Created in BioRender. **i** ChIP-qPCR for H3K9 acetylation (H3K9Ac) and H3K4 methylation (H3K4me) on *IGF1* promoter in hACs upon Wnt activation with LiCl (20 mM) for 24 h. **j** MACS2-binding scores in *IGF1* and *TCF1* promoters of publicly available TCF4, TCF3 and TCF1 ChIP-Seq data (ChIP-Atlas database). **b, c, f, g**  $n = 3$  different donors with 3 technical replicates per donor. Error bars indicate mean  $\pm$  SD. **(e, i)**  $n = 2$  different donors. **b, c, e, f, g, i** Source data are provided as a Source Data file.

**IGF1 silencing restores cell identity in diseased chondrocytes**

Finally, we evaluated the impact of decreasing IGF1 in articular chondrocytes from osteoarthritis patients, which exhibit increased Wnt signaling activation<sup>4</sup>. In these diseased chondrocytes, cell identity is lost, so that expression of healthy cartilage anabolic markers such as collagen 2a1 (COL2A1) and aggrecan (ACAN) is reduced, while expression of catabolic markers such as MMP13, ADAMTS4, and ADAMTS5 is often increased, compared to healthy cells<sup>29,30</sup>. Silencing of *IGF1* in hACs from osteoarthritis patients using siRNA increased expression of healthy markers *COL2A1* and *ACAN* and reduced expression of cartilage degrading enzymes *MMP13* and *ADAMTS4* and *5* (Fig. 6a–e and Supplementary Fig. 9d). Thus, siRNA-mediated targeting of *IGF1* favors the restoration of a healthy molecular profile in articular chondrocytes from osteoarthritis patients.

**Discussion**

In this study, we pinpoint IGF1 as a direct target gene of Wnt signaling in articular chondrocytes and demonstrate that its induction upon Wnt activation strongly contributes to the development and progression of osteoarthritis. These findings reveal an unknown regulatory and functional connection between two pivotal pathways in cartilage biology: Wnt signaling and the IGF1 axis (Fig. 6f). We conducted an unbiased bioinformatic analysis using datasets from Wnt hyperactivated articular cartilage. Coupling these with in vitro and in vivo experiments using primary human articular chondrocytes and cartilage-specific *Igf1*<sup>CART-KO</sup> mice, we unraveled that Wnt signaling transcriptionally induces IGF1, which drives detrimental joint changes in osteoarthritis. Furthermore, we identified the underlying molecular mechanisms: Wnt induction of IGF1 depends on  $\beta$ -catenin and subsequent binding of Wnt transcription factor TCF4 to the *IGF1* gene promoter. Crucially, we demonstrated the clinical relevance of our findings by showing proof of principle that deleting *Igf1* halts osteoarthritis in mice upon joint trauma. In addition, reducing IGF1 in articular chondrocytes from osteoarthritis patients restores a healthy molecular profile.

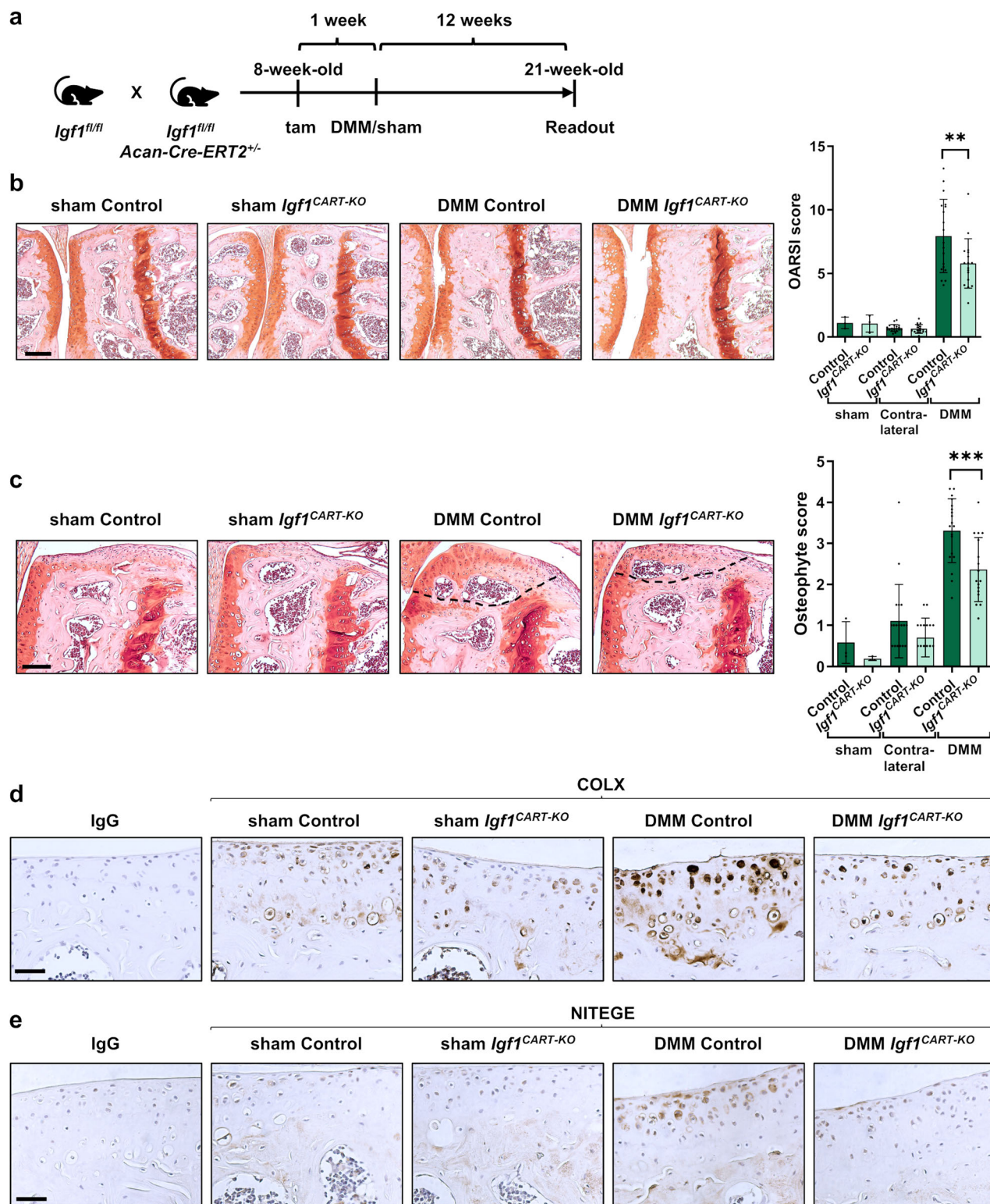
Excessive activation of Wnt signaling is strongly linked to the onset and severity of osteoarthritis<sup>5</sup>. In humans, genetic variants in the Wnt antagonist *FRZB*, various Wnt ligands, and different Wnt epigenetic modulators were associated with osteoarthritis<sup>31–34</sup>. Expression of Wnt activators and inhibitors was reported to respectively increase or decrease in articular cartilage, synovial tissue, and fluid from osteoarthritis patients<sup>35</sup>. In rodent models, loss of molecules that suppress Wnt signaling such as *Frzb*, *Dot1l*, and *Wnt16* resulted in increased osteoarthritis<sup>8,11,36</sup>. Consistent with these findings, the stabilization of  $\beta$ -catenin, leading to activation of Wnt signaling, induced osteoarthritis in mice<sup>4</sup>. Furthermore, mechanical injury was demonstrated to be a potent inducer of Wnt signaling in cartilage<sup>37</sup>. With such genetic and experimental evidence, Wnt signaling has been widely recognized as an appealing therapeutic target for osteoarthritis. Yet,

the downstream effects of Wnt signaling in cartilage remained underexplored, leading to a knowledge gap regarding effective and safe strategies for targeting this pathway. This includes uncertainty about which specific Wnt pathway components should be inhibited in osteoarthritis. Hence, understanding downstream molecular events upon Wnt signaling activation is a necessary step to achieve a higher degree of specificity in target definition. Our study provides important insights into a downstream molecular mechanism that is activated upon Wnt signaling, pinpointing IGF1 as a major effector of Wnt detrimental effects in osteoarthritis.

Polymorphisms in the *IGF1* and the *IGF1 receptor (IGF1R)* genes have been linked to osteoarthritis<sup>33,38–40</sup>. In growth plate cartilage, IGF1 plays a role in stimulating chondrocyte hypertrophy, promoting prenatal and postnatal bone growth<sup>15,16</sup>. However, the role of IGF1 in articular cartilage and osteoarthritis has remained controversial and largely undefined until now. Given its anabolic properties, IGF1 has been explored in tissue engineering approaches toward joint repair<sup>17</sup>. Nevertheless, recent reports showed that IGF1 can trigger aberrant chondrocyte hypertrophy in bovine articular chondrocytes<sup>18</sup> and in the human costal C28/I2 chondrocyte cell line<sup>19</sup>, thereby changing the cells' molecular identity. Our study provides unprecedented evidence on the role of IGF1 in osteoarthritis, revealing that IGF1 drives joint detrimental changes upon Wnt signaling activation and contributes to the onset and progression of the disease.

Two studies have reported experimental modulation of the *Igf1* gene in translational animal models of osteoarthritis. One of these studies examined the effects of adenovirus-mediated *IGF1* gene transfer in post-traumatic osteoarthritis in rabbits. However, the effects of IGF1 were evaluated in combination with basic fibroblast growth factor and an interleukin-1 receptor antagonist, making it challenging to discern the specific impact of IGF1 in the disease<sup>41</sup>. In another study, the role of liver-derived IGF1 in post-traumatic and spontaneous osteoarthritis was analyzed using liver-specific *Igf1* KO mice, which exhibited an approximate 80% reduction in circulating IGF1 levels. This study evidenced the limited impact of systemically produced IGF1 in osteoarthritis, and in agreement with our results, cartilage damage was not increased but slightly reduced in liver-specific *Igf1* KO mice<sup>42</sup>. Nevertheless, the role of locally produced IGF1 by articular cartilage in the initiation and progression of osteoarthritis has, until now, remained unexplored.

To our knowledge, this is the first study that investigates the role of IGF1 produced by articular chondrocytes in osteoarthritis using inducible cartilage-specific *Igf1* KO mice. Congenital whole-body *Igf1* KO mice exhibit severe growth retardation and, depending on their genetic background, mice die shortly after birth, while others can survive into adulthood<sup>43</sup>. Our research, encompassing both models of pharmacological Wnt hyper-activation and injury-induced osteoarthritis, revealed that *Igf1*<sup>CART-KO</sup> mice exhibited reduced cartilage damage, osteophytes, and suppressed chondrocyte hypertrophy and



aggrecan degradation when compared to control mice. These results demonstrate that deletion of the *Igf1* gene in articular cartilage protects against osteoarthritis in mice. Silencing of *IGF1* in articular chondrocytes from osteoarthritis patients contributed to the restoration of a healthy molecular profile. Our findings thus challenge the prevailing notion of IGF1 as a beneficial factor for cartilage health due to its anabolic properties. Instead, they emphasize that reducing IGF1, in response to Wnt signaling activation, represents a promising therapeutic strategy for osteoarthritis.

As we found IGF1 to be transcriptionally controlled by Wnt signaling, we focused on *Igf1* deletion in chondrocytes to evaluate the in vivo impact of our identified regulatory mechanism on osteoarthritis. Alternatively, cartilage-specific *Igf1r* KO mice could have been considered. However, IGF1R is not a specific receptor for IGF1 since it can also bind IGF2 and insulin<sup>44</sup>, and, furthermore, IGF1 does not exclusively bind to IGF1R on the cell surface<sup>44</sup>, thereby increasing the complexity of the research question. Further studies would be useful to define the role of IGF1R in osteoarthritis, and how

**Fig. 5 | Cartilage-specific deletion of *Igf1* protects against post-traumatic osteoarthritis in mice.** **a** Schematic outline of destabilization of the medial meniscus (DMM) or sham surgery after postnatal deletion of *Igf1* in male *Igf1<sup>CART-KO</sup>* mice. *Igf1<sup>fl/fl</sup>* mice were bred to *Igf1<sup>fl/fl</sup>;Aggrecan-Cre<sup>ERT2</sup>* and treated with tamoxifen. Tamoxifen-treated *Igf1<sup>fl/fl</sup>* mice served as controls. **b** Frontal haematoxylin-safraninO staining of the medial tibia and femur and quantification of articular cartilage damage at the 4 quadrants, evaluated by OARSI score. [*n* = 3 (sham control and sham *Igf1<sup>CART-KO</sup>*), *n* = 19 (DMM control) and *n* = 18 (DMM *Igf1<sup>CART-KO</sup>*)],  $F_{1,34} = 464.2, 7.419, 4.294$  for intervention, genotype and interaction, respectively, in two-way ANOVA comparing DMM and contralateral knees,  $**p = 0.0023$  for 2 pairwise tests using the Šidák multiple comparisons test. Error bars indicate mean ± SD. Scale bar: 200 μm.

**c** Frontal haematoxylin-safraninO staining of the medial tibia and quantification of osteophytes at the 4 quadrants. [*n* = 3 (sham control and sham *Igf1<sup>CART-KO</sup>*), *n* = 19 (DMM control) and *n* = 18 (DMM *Igf1<sup>CART-KO</sup>*)],  $F_{1,34} = 136.3, 12.67, 2.743$  for intervention, genotype and interaction, respectively, in two-way ANOVA comparing DMM and contralateral knees,  $***p = 0.0007$  for 2 pairwise tests using the Šidák multiple comparisons test. Error bars indicate mean ± SD. Scale bar: 100 μm. **b, c** Source data are provided as a Source Data file. **d, e** Immunohistochemical detection of hypertrophy marker collagen type 10 (COLX) (**d**) and aggrecan degradation marker NITEGE (**e**) in articular cartilage of *Igf1<sup>CART-KO</sup>* and control mice upon osteoarthritis triggered by DMM surgery compared with sham-operated mice (images are representative of 3–5 mice per group). Scale bar: 50 μm.

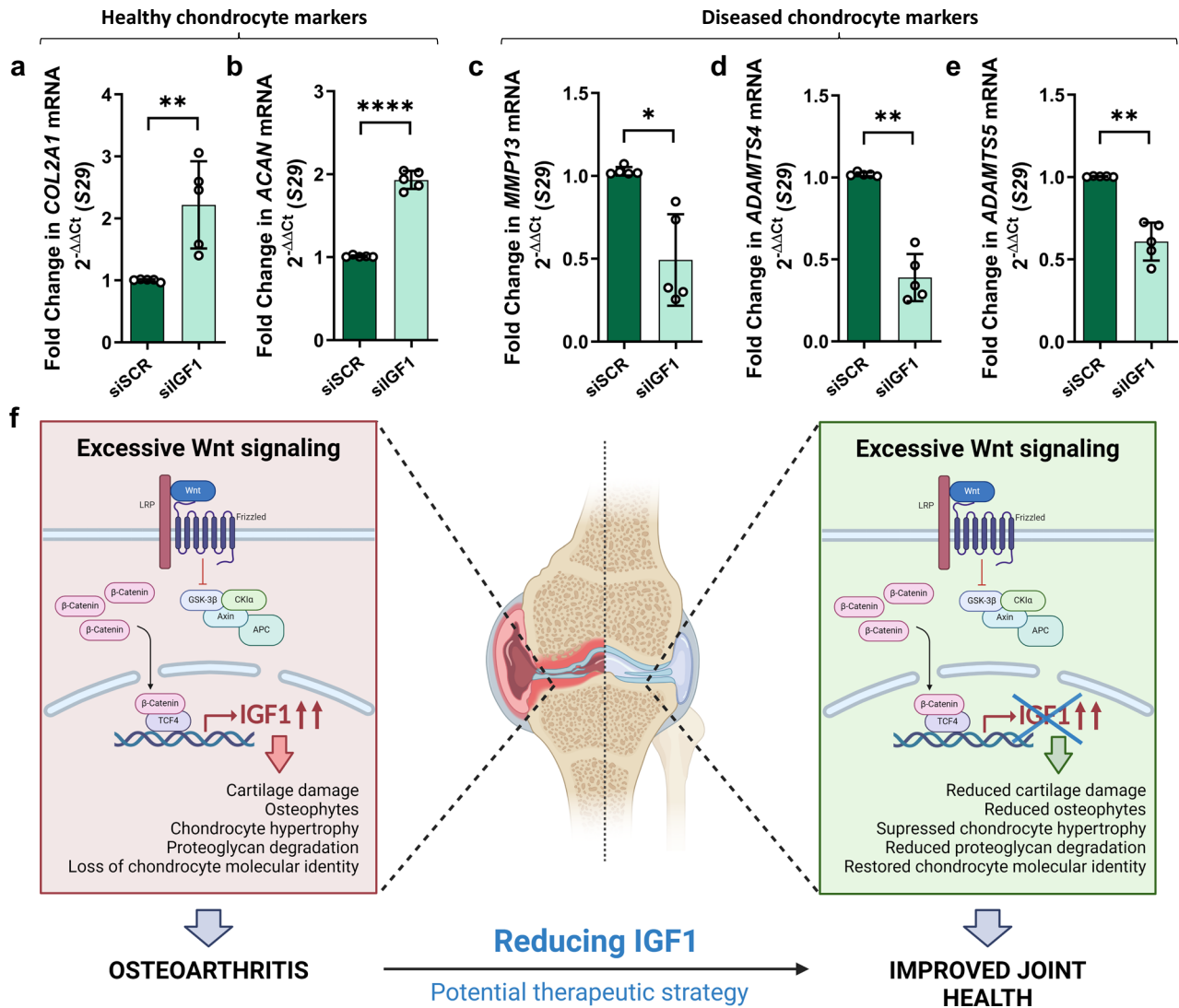


**Fig. 6 | Reducing IGF1 may be a therapeutic strategy for osteoarthritis.** **a–e** *IGF1* silencing restores a healthy molecular profile in articular chondrocytes from osteoarthritis patients. Real-time PCR of gene expression of healthy chondrocyte markers *COL2A1* (**a**) and *ACAN* (**b**), and of disease chondrocyte markers *MMP13* (**c**), *ADAMTS4* (**d**), and *ADAMTS5* (**e**) in human articular chondrocytes from osteoarthritis patients transfected with *IGF1* (siIGF1) or scramble control (siSCR) siRNA for 72 h (*n* = 5 different donors with 3 technical replicates per donor),  $**t_4 = 4.856, p = 0.0083$  (**a**);  $****t_4 = 22.41, p < 0.0001$  (**b**);  $*t_4 = 3.57, p = 0.0234$  (**c**);  $**t_4 = 6.534, p = 0.0028$  (**d**);

$**t_4 = 5.813, p = 0.0044$  (**e**) by two-sided paired *t*-test. Error bars indicate mean ± SD. Source data are provided as a Source Data file. **f** Conceptual summary of the main findings: Wnt signaling activation induces *IGF1* gene expression in articular chondrocytes, and this drives cartilage damage, osteophyte formation, chondrocyte hypertrophy, proteoglycan degradation and loss of chondrocyte molecular identity, leading to osteoarthritis. Reducing IGF1 upon Wnt activation in articular cartilage improves joint health with beneficial effects at multiple levels, representing a potential therapeutic strategy for osteoarthritis. Created in BioRender.

cartilage-specific deletion of *Igf1r* in mice impacts disease development and progression, as a next step to understand the effects of IGF1 and its complex downstream signaling in articular chondrocytes.

Our study reveals that Wnt signaling directly controls the transcription of IGF1 in articular chondrocytes, through a molecular mechanism that depends on β-catenin and binding of Wnt transcription factor TCF4 to the *IGF1* gene promoter. To date, the signaling

networks that control local IGF1 expression in articular cartilage remain unknown. Circulating IGF1 levels, primarily originating from the liver, are mainly regulated by GH<sup>45</sup>. GH-independent regulatory mechanisms of IGF1 expression were largely unexplored although these appear to be essential for controlling local IGF1 production in articular cartilage since GH does not increase IGF1 expression in articular chondrocytes, as we show here and as also previously reported<sup>21</sup>. Dore et al. demonstrated that, despite the presence of the GH receptor (GHR), adult human chondrocytes were unresponsive to GH stimulation regarding IGF1 production, as shown in dose-response and time-course studies<sup>21</sup>. Notably, we identify Wnt signaling as a key regulator of local IGF1 expression in articular cartilage.

Previous studies using animal models with altered GH levels or GHR dysfunction provided insights into the functions of GH in joint health but with mixed results. Zhu et al. reported that whole-body overexpression of bovine GH in mice predisposes to progressive joint degeneration while blocking GH action through systemic GH receptor disruption protects mice from developing age-associated osteoarthritis<sup>46</sup>. However, this study did not investigate the molecular mechanisms via which whole-body GH overexpression triggers joint degeneration. The authors speculated that their observations were caused directly by GH acting on articular cartilage, or indirectly via IGF1 (systemic or local), but no mechanism nor causality was examined. This research team recently reported that mice with deficient GH signaling through either germline or adult-induced *GHR* KO were protected from age-induced osteoarthritis<sup>47</sup>. Earlier studies examining hypopituitary dwarf mice reported that GH deficiency slows age-associated joint degeneration<sup>48,49</sup>. On the contrary, another study of dwarf rats reported increased severity of osteoarthritis<sup>50</sup>. In contrast, overexpression of bovine GH in mice increased cartilage clefts and synovial thickening at an early age<sup>51</sup>, suggesting increased GH action promotes osteoarthritis development. Another recent study using an inducible and isolated adult-onset GH deficiency mouse line showed that adult-onset reduction of GH increases osteoarthritis development<sup>52</sup>. The different and seemingly contradictory results from these studies make it difficult to draw conclusions about the impact of GH on the disease. And, importantly, the molecular mechanisms via which modulation of GH impacts joint health appear not to be demonstrated in these studies, and more in particular, no causal involvement of IGF1 was proven. Of note, GH can regulate a large range of signaling pathways besides the IGF1 axis<sup>53,54</sup>.

The identified Wnt/IGF1 regulatory mechanism may be relevant beyond cartilage biology and osteoarthritis. Our ChIP-Atlas analysis showed that TCF transcription factors bind to the *IGF1* gene promoter in various cell types besides chondrocytes, and our exploratory experiments in human fibroblasts and osteoblasts support this observation. Current literature indicates that Wnt signaling and IGF1 are simultaneously dysregulated and both play relevant roles in various human disorders, implying the possible involvement of a Wnt regulatory mechanism of IGF1. For instance, both Wnt signaling and IGF1 activation have been linked to the onset and progression of cardiac hypertrophy, which often leads to heart failure<sup>55,56</sup>. In numerous types of cancer, such as colorectal, Wnt signaling and IGF1 are aberrantly activated, initiating and driving tumor progression<sup>57,58</sup>. Also in the development of diabetes, dysregulations in Wnt signaling and IGF1 play determinant roles<sup>59,60</sup>. In Alzheimer's disease, loss of Wnt signaling has been demonstrated to contribute to neurodegeneration and cognitive decline<sup>61</sup>, and in parallel, lower serum IGF1 levels have been associated with this brain disorder<sup>62</sup>. Yet, no regulatory or functional link between Wnt signaling and IGF1 has been investigated in the mentioned diseases. Thus, our findings encourage specific investigation of the identified Wnt/IGF1 mechanistic link in diseases where both Wnt signaling and IGF1 are dysregulated and exploring its potential translational implications for disease management.

We acknowledge that this study has certain limitations. While we have verified that *Igf1*<sup>CART-KO</sup> mice have reduced IGF1 protein amounts in articular cartilage, it is possible that IGF1 from other sources such as systemically produced IGF1 or IGF1 produced by other joint cells, may still be present in the joint. In addition, while we have identified IGF1 as a key player in Wnt-triggered joint damage, we acknowledge the possible existence of other contributors that remain unidentified. Nevertheless, our findings demonstrate that cartilage-specific deletion of *Igf1* exerts protective effects in two mouse models of osteoarthritis, indicating the important contributing role of cartilage-produced IGF1 in Wnt-triggered joint disease. It is worth noting that, in our in vivo experiments, we exclusively used male mice due to their heightened susceptibility to osteoarthritis, as supported by previous studies<sup>63</sup>. Future studies would be needed to corroborate the role of IGF1 in osteoarthritis in female mice.

In summary, our study demonstrates that Wnt signaling directly induces the expression of IGF1 in articular cartilage and that IGF1 mediates detrimental effects of excessive Wnt signaling activation in the joint. Deletion of the *Igf1* gene in articular cartilage halts osteoarthritis after joint injury in mice, and silencing of *IGF1* in articular chondrocytes from osteoarthritis patients restores a healthy molecular profile. Therefore, our findings demonstrate that reducing IGF1 is a potential therapeutic strategy for osteoarthritis.

## Methods

### Study approval

Healthy primary human articular chondrocytes (hACs) were obtained from patients undergoing hip replacement for osteoporotic or malignancy-associated fractures, and chondrocytes from osteoarthritis patients were obtained after scheduled hip replacement surgery. Human osteoblasts were obtained from osteoarthritis hips and skin fibroblasts from abdominoplasty patients. The University Hospitals Leuven Ethics Committee and Biobank Committee (Leuven, Belgium) approved our studies, including the use of human biological residual material (hip joints and abdominal skin), which is exempt from the need to obtain written informed consent according to Belgian law and UZ Leuven's biobank policies. Patients are informed about this before surgery and can opt out. Only the age and sex of the patients were shared between the surgeons and the investigators involved in this study. Patient information is provided in Supplementary Data 1. All experiments with mice were approved by the Ethics Committee for Animal Research (P114-2008, P198-2012, P159-2016, P004-2022; KU Leuven).

### Study design

The objective of this study was to determine how excessive Wnt signaling activation causes joint destruction in osteoarthritis in humans and mice with particular attention to the downstream molecular effectors involved. Cells from patients with osteoarthritis and non-osteoarthritic controls were used in in vitro studies. Genetically engineered mice were used in different models of osteoarthritis. Mouse models are reported following the principles of the ARRIVE guidelines (Supplementary Table 4). For mouse experiments, the sample size was determined by a priori power analysis included in the Ethical approval request based on historical and simulated data using the partial eta-squared value to estimate the effect size. Our primary outcome is cartilage damage, scored on histological sections, based on OARSI guidelines<sup>64</sup>. In our experience and power analysis, we consider a 30% improvement biologically meaningful. The outcome was 8 ( $\alpha = 0.05 - \beta = 0.20$ ) or 9 mice ( $\alpha = 0.05 - \beta = 0.05$ ) respectively per group. Yet whereas 8 animals per group are sufficient for demonstrating the interaction between genotype and intervention, this setup may be underpowered for multiple post-hoc tests. Simulated data suggest that we need at least 12 mice in the CHIR groups and 8 mice in the control groups. For the DMM experiments, we decided to further increase our

sample size for the preclinical setup as genetic recombination within adult articular cartilage may not be uniform between animals. Because of our successful breeding plan with the genetically modified animals, we could include 19 and 18 animals in the DMM control and DMM *Igfl1<sup>CART-KO</sup>* groups, respectively. Disease severity end points were determined by pathology analysis. No exclusion of animals was carried out except for one extreme outlier in the DMM *Igfl1<sup>CART-KO</sup>* group (Supplementary Table 5). Mice were randomly assigned to the experimental groups where applicable. Pathology analysis was performed in a blinded way. For in vitro experiments, no a priori power calculation was performed. The setup was based on a convenience sample determined by the availability of primary human non-osteoarthritic or osteoarthritic cells.

## Materials

DOT1L inhibitor EPZ-5676 was obtained from Chemietek. Recombinant human WNT3A and GH proteins were purchased from R&D Systems. CHIR-99021 (CHIR) and lithium chloride (LiCl) were purchased from Sigma. XAV-939 (XAV) was purchased from Selleckem. Nontargeting siGENOME siRNA (siSCR) or siGENOME siRNA against  $\beta$ -catenin and IGF1 were purchased from Dharmacon. Nontargeting negative control siRNA (siSCR) or FlexiTube Gene Solution siRNA against TCF4 and TCF3 were purchased from Qiagen.

## Bioinformatic analysis

STRINGdb (<https://string-db.org>)<sup>9</sup> was used to explore protein-protein interactions and HumanBase (<https://hb.flatironinstitute.org>)<sup>10</sup> to examine cartilage-specific regulatory networks of top deregulated genes in datasets of Wnt hyper-activation in human chondrocytes or mouse cartilage previously generated in our research group (geonr: GSE77916 and GSE33656). The *IGF1* proximal promoter sequence 2400 bp upstream and 100 bp downstream relative to the TSS was obtained from the online tool EPD<sup>65</sup>, with the exception of the zebrafish *Igfl1* promoter that was obtained using the Ensemble Genome Browser ([www.ensembl.org](http://www.ensembl.org))<sup>66</sup>.

## Cell culture

For the isolation of primary hACs, cartilage was dissected from the joint surface, rinsed with PBS, and cut into small pieces. Cartilage explants were incubated with 2 mg/ml pronase solution (Roche) for 90 min at 37 °C under continuous agitation and digested overnight at 37 °C in 1.5 mg/ml collagenase B solution (Roche). The preparation was filtered through a 70  $\mu$ M strainer and cells were plated in culture flasks and cultured in a humidified atmosphere at 37 °C, 5% CO<sub>2</sub>. Culture medium consisted of DMEM/F12 (Gibco), 10% FBS (Gibco), 1% (vol/vol) antibiotic/antimycotic (Gibco), and 1% L-glutamine (Gibco).

Mouse C2C12 muscle cells (ATCC CRL-1772) were cultured in DMEM supplemented with 10% FBS and 1% penicillin and streptomycin at 37 °C in 5% CO<sub>2</sub>.

Primary human osteoblasts were isolated from the hips of patients undergoing total hip replacement surgery, using a modification of Beresford's procedure<sup>67</sup>. Trabecular bone was removed mechanically from the femur head, washed several times with sterile PBS to remove adherent cells, and cut into 2–4 mm<sup>2</sup> pieces. These explants were agitated in culture medium (1:1 mixture of DMEM and Ham's F-12 medium) (Gibco) containing 1% (vol/vol) antibiotic-antimycotic (Gibco), 10% FBS (Gibco) and 1% L-glutamine (Gibco), placed in a culture flask and incubated at 37 °C in a humidified atmosphere of 95% air and 5% CO<sub>2</sub>. To favor osteoblastic differentiation, the standard culture medium was supplemented with 100  $\mu$ g/ml ascorbic acid (Sigma) and 10 mM  $\beta$ -glycerophosphate (Sigma).

Human dermal fibroblasts were isolated from healthy human skin by enzymatic digestion using Dispase (4 mg/ml overnight 4 °C, Dispase II, Thermo Scientific), followed by mechanical removal of the epidermis and separation of the dermis into small pieces. The samples

were further digested with collagenase 1A in PBS (1 mg/ml, 2 h, 37 °C, Sigma Aldrich). Afterward, the preparation was filtered through a 70  $\mu$ M strainer and cells were plated in culture flasks and cultured in a humidified atmosphere at 37 °C, 5% CO<sub>2</sub>. Culture medium consisted of EMEM (Sigma Aldrich) supplemented with 15% FBS (Gibco), 1% (vol/vol) antibiotic/antimycotic (Gibco), 1% L-glutamine (Gibco), and 1% non-essential amino acids (Gibco). For the in vitro studies, cells at 80–90% confluency were treated with 3  $\mu$ M EPZ-5676, 100 ng/ml human WNT3A, 20 mM LiCl, and 3  $\mu$ M CHIR, unless otherwise indicated.

## RNA extraction, cDNA synthesis, and quantitative PCR analysis

Total RNA was extracted using the Nucleospin RNA II kit (Macherey-Nagel). cDNA was synthesized using the RevertAidHminus First Strand cDNA synthesis kit (Thermo Fisher Scientific) according to the manufacturers' recommendations. Quantitative PCR analyses were performed using the Maxima SYBRgreen qPCR master mix system (Thermo Fisher Scientific)<sup>7</sup>. Gene expression was calculated following normalization to housekeeping gene *S29* or *HPRT1* and analysis of gene expression was conducted using the 2<sup>- $\Delta\Delta$ CT</sup> method. The following PCR conditions were used: incubation for 10 min at 95 °C followed by 40 amplification cycles of 15 s of denaturation at 95 °C followed by 45 s of annealing-elongation at 60 °C. Melting curve analysis was performed to determine the specificity of the PCR. Primers used for qPCR analysis are listed in Supplementary Table 6.

## Mouse models

Wild-type male C57Bl/6 mice were purchased from Janvier (Le Genest St Isle, France). Mice were housed in groups of 4–5 mice in a Static micro-insulator cage with a Macrolon filter with bedding material (composed of spruce particles of approximately 2.5–3.5 mm, type Lignocel® BK 8/15), under conventional laboratory conditions (14 h light–10 h dark; 23  $\pm$  2 °C), with standard mouse chow food (Sniff, Soest, Germany) and water provided *ad libitum*.

*Dot1l* knockout (KO) mice were previously generated in our research group<sup>7,8</sup>. Congenital cartilage-specific *Dot1l* KO mice (*Dot1l<sup>CART-KO</sup>*) and inducible cartilage-specific *Dot1l* KO mice (*Dot1l<sup>CondCART-KO</sup>*) were used in this study. Knees from *Dot1l<sup>CART-KO</sup>* were harvested at 4 weeks of age and knees from *Dot1l<sup>CondCART-KO</sup>* were harvested at 21 weeks of age as reported in refs. 7,8.

*Frzb* KO mice were generated in our research group<sup>11</sup> and backcrossed into the C57Bl/6J background for over 10 generations. Wild-type littermates were used as controls. Knees from WT and *Frzb* KO male mice were harvested at 8 weeks of age.

Mice with exon 4 of the *Igfl1* gene flanked with *loxP* sites (B6.129(FVB)-*Igfl1<sup>tm1Dlr</sup>*/J; *Igfl1<sup>fl/fl</sup>*) were obtained from the Jackson Laboratory (Jax016831)<sup>68</sup>. *Igfl1<sup>fl/fl</sup>* were bred to *Aggrecan-Cre<sup>ERT2</sup>* (B6.Cg-*Acan<sup>tm1(cre/ERT2)Ccm</sup>*/J) mice (Jax019148)<sup>69</sup> (from Dr. G. Bou-Gharios and the Kennedy Institute, Oxford, UK) to generate inducible cartilage-specific *Igfl1* knockout mice (*Igfl1<sup>CART-KO</sup>*). Tamoxifen was injected intraperitoneally at the age of 8 weeks (1 mg/ml, 200  $\mu$ l, 3 injections, every other day)<sup>69</sup>, to activate the Cre recombinase activity of *Aggrecan-Cre<sup>ERT2</sup>* and delete *Igfl1* in cartilage. Tamoxifen-treated male littermates that were homozygous for *loxP* but lacked *Aggrecan-Cre<sup>ERT2</sup>* were used as controls; we refer to these mice as controls. Genotypes of animals were confirmed by PCR on genomic ear DNA as described<sup>68</sup>.

## EPZ-5676, XAV, and CHIR intra-articular injections

In vivo administration of DOT1L inhibitor EPZ-5676 and Wnt inhibitor XAV in wild-type mice was performed in our previous study<sup>7</sup>. Intra-articular administration of Wnt activator CHIR in wild-type, *Igfl1<sup>CART-KO</sup>*, and control mice was performed in different experiments. In a first setup aiming to assess changes in IGF1 protein amounts in articular cartilage, eight-week-old wild-type male C57Bl/6 mice were treated with an intra-articular injection of increasing doses of CHIR (1 mg/kg,

2.5 mg/kg, and 5 mg/kg) or vehicle (6% DMSO, 40% PEG400 in PBS), on day 1 and day 4. We estimated the concentration range of CHIR in this dose curve based on reported data<sup>70</sup>. PBS was injected into the left knee. The knees were harvested at 9 weeks of age. Next, we performed a pilot experiment in wild-type mice to determine empirically the dose and time regime of intra-articularly injected CHIR that induces osteoarthritis in mice. We tested a concentration of CHIR (5 mg/kg) based on histology observations in the dose curve experiment above, in two different regimes of administration (regime 1: four injections during two weeks; regime 2: six injections during two weeks; for both regimes: knees were harvested four weeks after the last injection). These timelines were based on our previous experience with osteoarthritis models upon intra-articular administration of pharmacological compounds<sup>7</sup>. In the final experiment, two weeks after injection of tamoxifen, 10-week-old *Igf1*<sup>CART-KO</sup>, and control mice were intra-articularly injected with CHIR (5 mg/kg) or vehicle (6% DMSO, 40% PEG400 in PBS) six times for two weeks, based on observations from the pilot experiment. PBS was injected into the left knee. The knees were harvested four weeks after the last injection, at 16 weeks of age.

### Histology

Dissected mouse knees were fixed overnight at 4 °C in 2% formaldehyde, decalcified for three weeks in 0.5 M EDTA pH 7.5, and embedded in paraffin. Hematoxylin-safraninO staining and immunohistochemistry were performed on 5 μm thick sections. The severity of the disease was determined by histological scores on Hematoxylin-safraninO stained sections throughout the knee by a blinded investigator (6 sections at 100 μm distance). Cartilage damage and synovial inflammation were assessed based on OARSI guidelines<sup>64</sup>. Depth of lesion (0–6) was scored on frontal knee sections. Lesion grades represent the following features; 0: surface and cartilage morphology intact, 1: small fibrillations without loss of cartilage, 2: vertical clefts below the superficial layer and some loss of surface lamina, 3–6: vertical clefts/erosions to the calcified cartilage extending, 3: less than 25%, 4: 25–50%, 5: 50–75% and 6: more than 75%. The score represents the sum of the means of four quadrants. For synovial inflammation, severity was determined on a 0–3 scale. Scoring grades for osteophytes represent the following features; 0: no osteophytes; 0.5: possible small osteophyte; 1: definite small osteophyte; 2: medium osteophyte; 3 large and mature osteophyte. Images were taken using a VisiTron Systems microscope (Leica Microsystems GmbH).

### Immunohistochemistry

Immunohistochemistry was performed on paraffin-embedded EDTA decalcified mouse knee sections. Heat-induced epitope retrieval was performed using a Citrate-EDTA buffer (pH 6.2) for 10 min at 95 °C. Next, sections were treated with 3% H<sub>2</sub>O<sub>2</sub>/methanol for 10 min to inactivate endogenous peroxidase activity, blocked in normal goat serum for 30 min, and incubated overnight at 4 °C with the primary antibodies against IGF1 (Abcam, ab9572; dilution 5 μg/ml), TCF1 (Abcam, ab96777; dilution 1:50), COLX (Abcam, ab58632; dilution 1:400), NITEGE (PAI-1746, Thermo Fisher Scientific; dilution 1:50), MMP13 (Abcam, ab39012, dilution 1:75) and ADAMT5 (Abcam, ab231595; dilution 4 μg/ml). Rabbit IgG (Santa Cruz, sc-2027) was used as a negative control. After incubation with the primary antibody, 1:100 biotin-conjugated-goat anti-rabbit (Vectastain ABC kit, Vector Laboratories) was applied for 30 min and DAB staining was used. For the detection of COLX and NITEGE, antigen retrieval was performed enzymatically with 10 mg/ml Hyaluronidase (Sigma Aldrich, H3884) in MgCl<sub>2</sub>-free PBS, for 40 min at 37 °C. In these cases, endogenous peroxidase activity was blocked after incubation with the primary antibody. For the detection of IGF1, no amplification was performed. Pictures were taken using a VisiTron Systems microscope (Leica Microsystems GmbH).

### Subchondral bone plate histomorphometry

Histomorphometry was performed on SafraninO stained sections using an Olympus IX83 microscope and digital image analysis using Osteomeasure software<sup>7,12</sup>. First, a box with a fixed width (800 μm) and variable height with the upper limit at the transition of calcified cartilage to the subchondral bone and the lower limit at the transition subchondral bone to growth plate was created from the digital image (referred to as subchondral bone area). Second, another box with the upper limit matched to the first box, and the lower limit at the transition of the subchondral bone plate to trabecular bone was generated (referred to as subchondral bone plate area). To correct for section artifacts, we do not show the subchondral bone plate surface area per se, but express the subchondral bone plate thickness as a ratio of the subchondral bone plate area to the subchondral bone area.

### IGF1 protein quantification ELISA

hACs were treated with different concentrations of WNT3A, CHIR, and LiCl for 24 h. The concentration of IGF1 in the cell culture supernatants was determined using an ELISA kit (ab100545), following the protocol provided by the manufacturer. This ELISA kit only detects the free form of human IGF1, it does not detect complexed or bound forms such as IGFBP-bound IGF1.

### Luciferase reporter assay

The full human IGF1 promoter sequence (–1999 bp to +100 bp relative to TSS) was amplified by PCR and cloned into the pGL3-Basic luciferase reporter vector (Promega, E1751) using the SmaI and HindIII sites (promoter sequence defined using EPD<sup>66</sup>). Primers used for the amplification are described in Supplementary Table 7. hACs were transfected with the full reporter plasmid using Lipofectamine LTX Reagent with PLUS Reagent (Invitrogen) according to the manufacturer's protocol. After 24 h, the cells were stimulated with WNT3A for 24 h. Luciferase assay was performed using Dual-Luciferase Reporter Assay System (Promega, E1910). The ratio of Firefly luciferase to Renilla luciferase (normalization control) was determined as relative luciferase activity.

### ChIP Analysis

ChIP assays were carried out using the Agarose ChIP kit (Thermo Fisher Scientific), according to the manufacturer's guidelines. Briefly, cell samples were cross-linked by 1% formaldehyde for 10 min, and the reaction was stopped by adding glycine to a 125 mM final concentration. The fixed cells were lysed in an SDS buffer, and the chromatin was fragmented by nuclease digestion. The sheared chromatin was incubated with antibodies against TCF1 (Cell signaling, #2203; dilution 1:50), TCF3 (Cell signaling #2883; dilution 1:50), TCF4 (Cell signaling, #2569; dilution 1:50), LEF1 (Merck Millipore, 17-604; dilution 1:50), H3K9ac (Abcam, Ab4441; dilution 1:125), H3K4me3 (Abcam, ab8580; dilution 1:100) and recovered by binding to protein A/G agarose. Eluted DNA fragments were used directly for qPCR. Primers used for ChIP-qPCR analysis are listed in Supplementary Table 8.

In silico ChIP analysis was performed using the ChIP-Atlas (<https://chip-atlas.org>)<sup>26</sup>, an integrative and comprehensive data-mining suite of public ChIP-Seq data. The feature Target Genes were used to predict target genes bound by TCF1, TCF3, and TCF4 transcription factors. The peak-caller Model-based Analysis of the ChIP-Seq (MACS2) algorithm captures the influence of genome complexity to evaluate the significance of enriched ChIP regions. These MACS2-binding significance scores were evaluated for *IGF1* and *TCF1* gene promoters in each individual ChIP-Seq experiment. Finally, BigWig data of TCF1, TCF3, and TCF4 ChIP-Seq performed in several cell types were visualized in the *IGF1* and *TCF1* gene promoters. All the data were mapped to the reference human genome (hg19) using the Integrative Genomics Viewer. Our analyses included the following publicly available ChIP-Atlas datasets: SRX1491250, SRX220960, SRX702131, SRX702105,

SRX096349, SRX096350, SRX2661484, SRX190201, SRX656347, SRX236115, SRX2043230, SRX158106, SRX4017892, SRX5794309.

### Small interfering RNA transfection

Cells were transfected with Lipofectamine RNAiMAX (Invitrogen) as transfection reagent, together with 20 nM of the corresponding siRNA for 72 h, following the manufacturer's instructions.

### Post-traumatic mouse model of osteoarthritis

At 9 weeks of age, post-traumatic osteoarthritis was induced by destabilization of the medial meniscus (DMM). To this end, a mild instability of the knee was obtained by surgical transection of the medial menisco-tibial ligament of the right knee<sup>27</sup>. Sham surgery was performed as a negative control. The left knees were left intact and used as control; we refer to these as contralateral knees. The knees were histologically analyzed 12 weeks after surgery. All mice studies were performed on male mice due to previous studies demonstrating an increase in osteoarthritis severity in male mice upon DMM compared to female mice<sup>63</sup>.

### Statistical analysis

Data analysis and graphical presentation were performed with GraphPad Prism version 10.0.3. All tests applied were 2-tailed. For comparisons between two groups with non-independent data, paired Student's *t*-test was used. For comparisons between more than two groups, one-way or two-way analysis of variance (ANOVA) was used with repeated measures in case of non-independence of data points. Dunnett and Šidák corrections were used for multiple comparisons. Data distribution and homogeneity of variance were assessed by data type, visual inspection of residual plots (residuals, QQ plots), and Shapiro–Wilk tests where applicable. Models were improved by data-transformation (log or square-root) where necessary. Effect sizes and model assumptions (residuals, QQ plots, Shapiro–Wilk test) for the analyses are presented in Supplementary Fig. 16. Analysis outcomes are reported by *p* values (significance <0.05). Data are presented as individual data points in the graph, representing the mean of biological or technical replicates, as indicated in the figure legends. Summary values presented in the graphs are the mean and associated standard deviation (SD).

### Reporting summary

Further information on research design is available in the Nature Portfolio Reporting Summary linked to this article.

### Data availability

Microarray data that were used in this study were deposited in Gene Expression Omnibus with the primary accession codes [GSE77916](https://www.ncbi.nlm.nih.gov/geo/query/acc.cgi?acc=GSE77916) and [GSE33656](https://www.ncbi.nlm.nih.gov/geo/query/acc.cgi?acc=GSE33656). The authors declare that all other data supporting the findings of this study are available within the article and its supplementary files. Source data are provided with this paper.

### References

- Hunter, D. J., March, L. & Chew, M. Osteoarthritis in 2020 and beyond: a Lancet Commission. *Lancet* **396**, 1711–1712 (2020).
- Osteoarthritis: a serious disease, submitted to the U.S. Food and Drug Administration <https://oarsi.org/oarsi-white-paper-oa-serious-disease> (2016).
- Conaghan, P. G., Kloppenburg, M., Schett, G. & Bijlsma, J. W. Osteoarthritis research priorities: a report from a EULAR ad hoc expert committee. *Ann. Rheum. Dis.* **73**, 1442–1445 (2014).
- Zhu, M. et al. Activation of beta-catenin signaling in articular chondrocytes leads to osteoarthritis-like phenotype in adult beta-catenin conditional activation mice. *J. Bone Min. Res.* **24**, 12–21 (2009).
- Monteagudo, S. & Lories, R. J. Cushioning the cartilage: a canonical Wnt restricting matter. *Nat. Rev. Rheumatol.* **13**, 670–681 (2017).
- Lories, R. J. & Monteagudo, S. Review article: is Wnt signaling an attractive target for the treatment of osteoarthritis? *Rheumatol. Ther.* **7**, 259–270 (2020).
- Monteagudo, S. et al. DOT1L safeguards cartilage homeostasis and protects against osteoarthritis. *Nat. Commun.* **8**, 15889 (2017).
- Cornelis, F. M. F. et al. Increased susceptibility to develop spontaneous and post-traumatic osteoarthritis in Dot1l-deficient mice. *Osteoarthr. Cartil.* **27**, 513–525 (2019).
- Szklarczyk, D. et al. STRING v11: protein-protein association networks with increased coverage, supporting functional discovery in genome-wide experimental datasets. *Nucleic Acids Res.* **47**, D607–d613 (2019).
- Greene, C. S. et al. Understanding multicellular function and disease with human tissue-specific networks. *Nat. Genet.* **47**, 569–576 (2015).
- Lories, R. J. et al. Articular cartilage and biomechanical properties of the long bones in Frzb-knockout mice. *Arthritis Rheum.* **56**, 4095–4103 (2007).
- Thysen, S., Luyten, F. P. & Lories, R. J. Loss of Frzb and Sfrp1 differentially affects joint homeostasis in instability-induced osteoarthritis. *Osteoarthr. Cartil.* **23**, 275–279 (2015).
- Lodewyckx, L., Cailotto, F., Thysen, S., Luyten, F. P. & Lories, R. J. Tight regulation of wingless-type signaling in the articular cartilage - subchondral bone biomechanical unit: transcriptomics in Frzb-knockout mice. *Arthritis Res. Ther.* **14**, R16 (2012).
- Philippou, A., Maridaki, M., Pneumaticos, S. & Koutsilieris, M. The complexity of the IGF1 gene splicing, posttranslational modification and bioactivity. *Mol. Med.* **20**, 202–214 (2014).
- Wang, J., Zhou, J. & Bondy, C. A. Igf1 promotes longitudinal bone growth by insulin-like actions augmenting chondrocyte hypertrophy. *FASEB J.* **13**, 1985–1990 (1999).
- Cooper, K. L. et al. Multiple phases of chondrocyte enlargement underlie differences in skeletal proportions. *Nature* **495**, 375–378 (2013).
- Wen, C. et al. Insulin-like growth factor-1 in articular cartilage repair for osteoarthritis treatment. *Arthritis Res Ther.* **23**, 277 (2021).
- Müller, S., Lindemann, S. & Gigout, A. Effects of sprifermin, IGF1, IGF2, BMP7, or CNP on bovine chondrocytes in monolayer and 3D culture. *J. Orthop. Res.* **38**, 653–662 (2020).
- Repudi, S. R., Patra, M. & Sen, M. WISP3-IGF1 interaction regulates chondrocyte hypertrophy. *J. Cell Sci.* **126**, 1650–1658 (2013).
- Wallis, M. New insulin-like growth factor (IGF)-precursor sequences from mammalian genomes: the molecular evolution of IGFs and associated peptides in primates. *Growth Horm. IGF Res.* **19**, 12–23 (2009).
- Doré, S. et al. Increased insulin-like growth factor 1 production by human osteoarthritic chondrocytes is not dependent on growth hormone action. *Arthritis Rheum.* **38**, 413–419 (1995).
- Singh, P., Marcu, K. B., Goldring, M. B. & Otero, M. Phenotypic instability of chondrocytes in osteoarthritis: on a path to hypertrophy. *Ann. N. Y. Acad. Sci.* **1442**, 17–34 (2019).
- Cadigan, K. M. & Waterman, M. L. TCF/LEFs and Wnt signaling in the nucleus. *Cold Spring Harb. Perspect. Biol.* **4**, 11 (2012).
- Ramakrishnan, A. B. & Cadigan, K. M. Wnt target genes and where to find them. *F1000Res* **6**, 746 (2017).
- Ma, B., Zhong, L., van Blitterswijk, C. A., Post, J. N. & Karperien, M. T cell factor 4 is a pro-catabolic and apoptotic factor in human articular chondrocytes by potentiating nuclear factor κB signaling. *J. Biol. Chem.* **288**, 17552–17558 (2013).
- Oki, S. et al. ChIP-Atlas: a data-mining suite powered by full integration of public ChIP-seq data. *EMBO Rep.* **19**, 12 (2018).

27. Glasson, S. S., Blanchet, T. J. & Morris, E. A. The surgical destabilization of the medial meniscus (DMM) model of osteoarthritis in the 129/SvEv mouse. *Osteoarthr. Cartil.* **15**, 1061–1069 (2007).
28. Lietman, C. et al. Inhibition of Wnt/ $\beta$ -catenin signaling ameliorates osteoarthritis in a murine model of experimental osteoarthritis. *JCI Insight* **3**, 3 (2018).
29. Goldring, S. R. & Goldring, M. B. Changes in the osteochondral unit during osteoarthritis: structure, function and cartilage-bone cross-talk. *Nat. Rev. Rheumatol.* **12**, 632–644 (2016).
30. Jiang, L. et al. ADAMTS5 in osteoarthritis: biological functions, regulatory network, and potential targeting therapies. *Front. Mol. Biosci.* **8**, 703110 (2021).
31. Loughlin, J. et al. Functional variants within the secreted frizzled-related protein 3 gene are associated with hip osteoarthritis in females. *Proc. Natl Acad. Sci. USA* **101**, 9757–9762 (2004).
32. Castaño Betancourt, M. C. et al. Genome-wide association and functional studies identify the DOT1L gene to be involved in cartilage thickness and hip osteoarthritis. *Proc. Natl Acad. Sci. USA* **109**, 8218–8223 (2012).
33. Boer, C. G. et al. Deciphering osteoarthritis genetics across 826,690 individuals from 9 populations. *Cell* **184**, 4784–4818.e4717 (2021).
34. Boer, C. G. et al. Genome-wide association of phenotypes based on clustering patterns of hand osteoarthritis identify WNT9A as novel osteoarthritis gene. *Ann. Rheum. Dis.* **80**, 367–375 (2021).
35. Zhou, Y., Wang, T., Hamilton, J. L. & Chen, D. Wnt/ $\beta$ -catenin signaling in osteoarthritis and in other forms of arthritis. *Curr. Rheumatol. Rep.* **19**, 53 (2017).
36. Nalesso, G. et al. WNT16 antagonises excessive canonical WNT activation and protects cartilage in osteoarthritis. *Ann. Rheum. Dis.* **76**, 218–226 (2017).
37. Dell'Accio, F., De Bari, C., Eltawil, N. M., Vanhummelen, P. & Pitzalis, C. Identification of the molecular response of articular cartilage to injury, by microarray screening: Wnt-16 expression and signaling after injury and in osteoarthritis. *Arthritis Rheum.* **58**, 1410–1421 (2008).
38. Meulenbelt, I. et al. A genetic association study of the IGF-1 gene and radiological osteoarthritis in a population-based cohort study (the Rotterdam Study). *Ann. Rheum. Dis.* **57**, 371–374 (1998).
39. Zhai, G. et al. Insulin-like growth factor I gene promoter polymorphism, collagen type II alpha1 (COL2A1) gene, and the prevalence of radiographic osteoarthritis: the Rotterdam Study. *Ann. Rheum. Dis.* **63**, 544–548 (2004).
40. Urano, T. et al. Association of a single nucleotide polymorphism in the insulin-like growth factor-1 receptor gene with spinal disc degeneration in postmenopausal Japanese women. *Spine* **33**, 1256–1261 (2008).
41. Chen, B., Qin, J., Wang, H., Magdalou, J. & Chen, L. Effects of adenovirus-mediated bFGF, IL-1Ra and IGF-1 gene transfer on human osteoarthritic chondrocytes and osteoarthritis in rabbits. *Exp. Mol. Med.* **42**, 684–695 (2010).
42. Törnqvist, A. E., Sophocleous, A., Ralston, S. H., Ohlsson, C. & Svensson, J. Liver-derived IGF-I is not required for protection against osteoarthritis in male mice. *Am. J. Physiol. Endocrinol. Metab.* **317**, E1150–e1157 (2019).
43. Kineman, R. D., Del Rio-Moreno, M. & Sarmiento-Cabral, A. 40 YEARS of IGF1: understanding the tissue-specific roles of IGF1/IGF1R in regulating metabolism using the Cre/loxP system. *J. Mol. Endocrinol.* **61**, T187–t198 (2018).
44. Aguirre, G. A., González-Guerra, J. L., Espinosa, L. & Castilla-Cortazar, I. Insulin-like growth factor 1 in the cardiovascular system. *Rev. Physiol. Biochem. Pharmacol.* **175**, 1–45 (2018).
45. Mukherjee, A., Alzhanov, D. & Rotwein, P. Defining human insulin-like growth factor I gene regulation. *Am. J. Physiol. Endocrinol. Metab.* **311**, E519–E529 (2016).
46. Zhu, S. et al. Promotion of joint degeneration and chondrocyte metabolic dysfunction by excessive growth hormone in mice. *Arthritis Rheumatol.* **75**, 1139–1151 (2023).
47. Liu, H. et al. Growth hormone-receptor disruption in mice reduces osteoarthritis and chondrocyte hypertrophy. *Geroscience* **46**, 4895–4908 (2024).
48. Silberberg, R. Articular aging and osteoarthrosis in dwarf mice. *Pathol. Microbiol.* **38**, 417–430 (1972).
49. Ewart, D. et al. Naturally occurring osteoarthritis in male mice with an extended lifespan. *Connect Tissue Res.* **61**, 95–103 (2020).
50. Ekenstedt, K. J., Sonntag, W. E., Loeser, R. F., Lindgren, B. R. & Carlson, C. S. Effects of chronic growth hormone and insulin-like growth factor 1 deficiency on osteoarthritis severity in rat knee joints. *Arthritis Rheum.* **54**, 3850–3858 (2006).
51. Vijayakumar, A., Yakar, S. & Leroith, D. The intricate role of growth hormone in metabolism. *Front. Endocrinol.* **2**, 32 (2011).
52. Poudel, S. B. et al. Sexual dimorphic impact of adult-onset somatopause on life span and age-induced osteoarthritis. *Aging Cell* **20**, e13427 (2021).
53. Dehkhoda, F., Lee, C. M. M., Medina, J. & Brooks, A. J. The growth hormone receptor: mechanism of receptor activation, cell signaling, and physiological aspects. *Front. Endocrinol.* **9**, 35 (2018).
54. Lu, M., Flanagan, J. U., Langley, R. J., Hay, M. P. & Perry, J. K. Targeting growth hormone function: strategies and therapeutic applications. *Signal Transduct. Target Ther.* **4**, 3 (2019).
55. Bergmann, M. W. WNT signaling in adult cardiac hypertrophy and remodeling: lessons learned from cardiac development. *Circ. Res.* **107**, 1198–1208 (2010).
56. Duerr, R. L. et al. Insulin-like growth factor-1 enhances ventricular hypertrophy and function during the onset of experimental cardiac failure. *J. Clin. Invest.* **95**, 619–627 (1995).
57. Zhao, H. et al. Wnt signaling in colorectal cancer: pathogenic role and therapeutic target. *Mol. Cancer* **21**, 144 (2022).
58. Vigneri, P. G. et al. The insulin/IGF system in colorectal cancer development and resistance to therapy. *Front. Oncol.* **5**, 230 (2015).
59. Chen, J. et al. Role of Wnt signaling pathways in type 2 diabetes mellitus. *Mol. Cell Biochem.* **476**, 2219–2232 (2021).
60. Biadgo, B., Tamir, W. & Ambachew, S. Insulin-like growth factor and its therapeutic potential for diabetes complications - mechanisms and metabolic links: a review. *Rev. Diabet. Stud.* **16**, 24–34 (2020).
61. Tapia-Rojas, C. & Inestrosa, N. C. Loss of canonical Wnt signaling is involved in the pathogenesis of Alzheimer's disease. *Neural Regen. Res.* **13**, 1705–1710 (2018).
62. Westwood, A. J. et al. Insulin-like growth factor-1 and risk of Alzheimer dementia and brain atrophy. *Neurology* **82**, 1613–1619 (2014).
63. Ma, H. L. et al. Osteoarthritis severity is sex dependent in a surgical mouse model. *Osteoarthr. Cartil.* **15**, 695–700 (2007).
64. Glasson, S. S., Chambers, M. G., Van Den Berg, W. B. & Little, C. B. The OARSI histopathology initiative - recommendations for histological assessments of osteoarthritis in the mouse. *Osteoarthr. Cartil.* **18**, S17–S23 (2010).
65. Dreos, R., Ambrosini, G., Périer, R. C. & Bucher, P. The Eukaryotic Promoter Database: expansion of EPDnew and new promoter analysis tools. *Nucleic Acids Res.* **43**, D92–D96 (2015).
66. Cunningham, F. et al. Ensembl 2022. *Nucleic Acids Res.* **50**, D988–D995 (2022).
67. Beresford, J. N., Gallagher, J. A., Poser, J. W. & Russell, R. G. Production of osteocalcin by human bone cells in vitro. Effects of 1,25(OH)2D3, 24,25(OH)2D3, parathyroid hormone, and glucocorticoids. *Metab. Bone Dis. Relat. Res.* **5**, 229–234 (1984).
68. Liu, J. L. et al. Insulin-like growth factor-I affects perinatal lethality and postnatal development in a gene dosage-dependent manner: manipulation using the Cre/loxP system in transgenic mice. *Mol. Endocrinol.* **12**, 1452–1462 (1998).

69. Lo, C. et al. Generation of a mouse line harboring a Bi-transgene expressing luciferase and tamoxifen-activatable creER(T2) recombinase in cartilage. *Genesis* **52**, 110–119 (2014).
70. Litherland, G. J. et al. Glycogen synthase kinase 3 inhibition stimulates human cartilage destruction and exacerbates murine osteoarthritis. *Arthritis Rheumatol.* **66**, 2175–2187 (2014).

## Acknowledgements

We are grateful to L. Storms and A. Hens for their technical support of this study and for taking care of the animal facility management. We are indebted to the UZ Leuven traumatology and orthopedics nursing staff for their efforts to provide cartilage samples for ex vivo and in vitro work. This work was supported by grants from the Flanders Research Foundation (FWO-Vlaanderen): G097118N (R.L.), G056822N (S.M.), and G059223N (S.M.). A.E.N. is the recipient of a fundamental research PhD fellowship from FWO-Vlaanderen (11L1822N). A.D.R. is the recipient of a junior postdoctoral fellowship from FWO-Vlaanderen (12AMS24N).

## Author contributions

S.M., R.J.L., and A.E.N. planned the study and designed all the in vitro, ex vivo, and in vivo experiments. A.E.N., S.M., and A.D.R. performed in vitro and ex vivo experiments. FMFC performed the animal experiments. F.C. cloned and provided the plasmid constructs for the luciferase assay. R.J.L. and A.E.N. are responsible for all statistical analyses. A.S. provided essential materials. S.M., A.E.N., and R.J.L. wrote the manuscript.

## Competing interests

Leuven Research and Development, the technology transfer office of KU Leuven, has received consultancy and speaker fees and research grants on behalf of R.J.L. from Abbvie, Boehringer-Ingelheim, Amgen (formerly Celgene), Eli-Lilly, Galapagos, Janssen, Fresenius Kabi, MSD, Novartis, Pfizer, Biosplice Therapeutics (formerly Samumed), Biocon (formerly Viatrix), UCB. None of these are directly related to the work presented here. The other authors declare no competing interests.

## Additional information

**Supplementary information** The online version contains supplementary material available at <https://doi.org/10.1038/s41467-024-53604-8>.

**Correspondence** and requests for materials should be addressed to Silvia Monteagudo.

**Peer review information** *Nature Communications* thanks the anonymous reviewers for their contribution to the peer review of this work. A peer review file is available.

**Reprints and permissions information** is available at <http://www.nature.com/reprints>

**Publisher's note** Springer Nature remains neutral with regard to jurisdictional claims in published maps and institutional affiliations.

**Open Access** This article is licensed under a Creative Commons Attribution-NonCommercial-NoDerivatives 4.0 International License, which permits any non-commercial use, sharing, distribution and reproduction in any medium or format, as long as you give appropriate credit to the original author(s) and the source, provide a link to the Creative Commons licence, and indicate if you modified the licensed material. You do not have permission under this licence to share adapted material derived from this article or parts of it. The images or other third party material in this article are included in the article's Creative Commons licence, unless indicated otherwise in a credit line to the material. If material is not included in the article's Creative Commons licence and your intended use is not permitted by statutory regulation or exceeds the permitted use, you will need to obtain permission directly from the copyright holder. To view a copy of this licence, visit <http://creativecommons.org/licenses/by-nc-nd/4.0/>.

© The Author(s) 2024